NCB-M31936C

An Apical MRCK-driven Morphogenetic Pathway Controls Epithelial Polarity

Ceniz Zihni[1], Evi Vlassaks[2,7], Stephen Terry[1,6], Jeremy Carlton[3], Thomas King Chor Leung[4] Michael Olson[5], Franck Pichaud[2], Maria Susana Balda[1,8], Karl Matter[1,8]

[1] Institute of Ophthalmology, University College London, Bath Street, London EC1V 9EL, UK
[2] MRC Laboratory for Molecular Cell Biology, University College London, Gower Street, London WC1E 6BT, UK
[3] Division of Cancer Studies, Section of Cell Biology and Imaging, King's College London, London SE1 1UL, UK
[4] Institute of Molecular and Cell Biology, A-STAR, 61 Biopolis Drive, Singapore 138673 and the Department of Anatomy, National University of Singapore, Singapore 119260, Singapore.
[5] Cancer Research UK Beatson Institute, Garscube Estate, Switchback Road, Glasgow G61 1BD, UK
[6] Current Address: Randall Division of Cell and Molecular Biophysics, King's College London, SE1 1UL, UK
[7] Current Address: Faculty of Life Sciences, University of Manchester, Oxford Road, Manchester, M13 9PT, UK
[8] Correspondence should be addressed to Karl Matter (k.matter@ucl.ac.uk) or Maria Susana Balda (m.balda@ucl.ac.uk)

Polarized epithelia develop distinct cell surface domains, with the apical membrane acquiring characteristic morphological features such as microvilli. Cell polarization is driven by polarity determinants including the evolutionarily conserved partitioning defective (PAR) proteins that are separated into distinct cortical domains. PAR protein segregation is thought to be a consequence of asymmetric actomyosin contractions. The mechanism of activation of apically polarized actomyosin contractility is unknown. Here we show that the Cdc42 effector MRCK activates Myosin-II at the apical pole to segregate aPKC-Par6 from junctional Par3, defining the apical domain. Apically polarized MRCK-activated actomyosin contractility is reinforced by cooperation with aPKC-Par6 downregulating antagonistic RhoA-driven junctional actomyosin contractility, and drives polarization of cytosolic brush border determinants and apical morphogenesis. MRCK-activated polarized actomyosin contractility is required for apical differentiation and morphogenesis in vertebrate epithelia and *Drosophila* photoreceptors. Our results identify an apical origin of actomyosin-driven morphogenesis that couples cytoskeletal reorganization to PAR polarity signalling.

Epithelial cells polarize and form distinct cell surface domains that have different biochemical compositions, reflecting their different functions[1]. The apical domain often undergoes a morphogenetic process leading to the development of actin-rich structures that support specific apical functions, such as the brush border membrane of absorptive epithelia or the light-harvesting domain of Drosophila photoreceptors. Formation of such apical specializations relies on the recruitment of specific cytosolic factors that determine apical morphogenesis and, hence, requires asymmetric distribution of cytosolic components[2]. Epithelial polarization is regulated by apical and basolateral polarity determinants[3]. Among which are the evolutionarily conserved PAR proteins that segregate into two distinct cortical domains[4, 5]. In epithelia, the boundary between the two domains, the apical/lateral border (tight junctions in vertebrates, adherens junctions in flies), is marked by Par3, which is recruited to the cell surface bound to the Par6-aPKC complex. In response to apical Cdc42 activation, Par3 dissociates, demarking the apical/lateral border, and the Par6-aPKC complex segregates into the differentiating apical domain[6, 7]. Studies in *C. elegans* one-cell stage embryos suggest that PAR protein segregation relies on asymmetric actomyosin activity, generating movement of anterior PAR complexes to the anterior pole, which results in the formation of two cortical domains that harbour distinct PAR proteins[8-13]. Anterior PAR proteins correspond to apical PARs in epithelia. The functional importance of actomyosin and, if relevant, how and where asymmetric Myosin-II activity is generated to drive apical accumulation of PAR proteins in epithelia is not clear. Identifying such mechanisms, however, is essential to understand how the interplay between mechanical forces generated by actomyosin contractility and biochemical signalling guide epithelial polarization and morphogenesis.

In epithelia, RhoA is known to generate contractile forces driving junction formation and remodelling, a mechanism important during apical constriction and developmental processes requiring epithelial sheet movement and elongation[14-16]. In contrast, apical Cdc42 activation not only drives apical differentiation but also promotes apical expansion at the cost of the basolateral domain, counteracting junctional actomyosin-generated apical constriction[17]. In

analogy to the *C. elegans* embryo model, one would expect a mechanism of Myosin-II activation at the apical pole to create an actomyosin activity gradient that favours apical polarization if apical segregation of Par6-aPKC is indeed driven by actomyosin contractions. Therefore, we asked if and how apical Cdc42 signalling activates asymmetric actomyosin contractility to stimulate apical polarization and plasma membrane morphogenesis, and how such a mechanism interacts with counteracting junctional RhoA signalling. Here, we show that the Cdc42 effector MRCK activates apical actomyosin contractility, initiating a pathway regulating apical morphogenesis, and cooperates with the aPKC-Par6 complex, which downregulates RhoA-driven junctional actomyosin contractility, to drive apical polarization.

RESULTS

MRCK-activated Myosin-II drives apical morphogenesis

As epithelial cells polarize and develop a specialized apical membrane domain, Myosin-II polarizes apically at distinct sites along the apical membrane domain including the junctional circumferential actomyosin belt[18, 19]. In cultured canine kidney epithelial MDCK cells that spontaneously differentiate, we found that phosphorylated MLC (myosin regulatory light chain), demarking active Myosin-II, is localised basolaterally in non-polarized cells and becomes increasingly enriched along the apical membrane domain, forming 'caps' that define the apical cellular cortex, as epithelial cells polarize and differentiate over a period of a few days (Fig.1a). Since apical polarization of PAR proteins and morphogenesis depends on apically polarized Cdc42 activation[3, 20], we asked whether a Cdc42-dependent mechanism driving polarized Myosin-II activation is at the origin of apical polarization and morphogenesis.

MRCKs are Cdc42 effector kinases that activate Myosin-II by phosphorylating MLC[21]. Using spontaneously differentiating MDCK cells, we asked whether siRNA-mediated MRCK knockdown affected formation of apical actomyosin caps. Indeed, MRCK depleted cells failed to form differentiated apical membranes as microvilli did not assemble, apical accumulation of F-actin and active Myosin-II did not occur, and had a reduced cell height (Fig. 1b-h, Supplementary Fig. 1a-c). All of these MRCK siRNA-induced effects were rescued by expression of siRNA resistant MRCKβ-flag, supporting specificity. MRCK was also required for the differentiation of human intestinal epithelial Caco-2 cells that also spontaneously polarize and differentiate (Supplementary Fig. 1c,d). Hence, MRCK is essential for the differentiation of vertebrate epithelial cells from different tissues.

To determine whether MRCK-generated apical Myosin-II activation is a conserved mechanism, we turned to *D.* melanogaster: their differentiating photoreceptors represent a well-characterized invertebrate model system to study epithelial polarity, PAR polarity signalling, and apical differentiation[5, 7, 22-24]. Drosophila photoreceptors undergo epithelial polarity remodelling during retinal development and evolve a characteristic, F-actin-rich apical membrane domain (Fig. 2a). Strikingly, differentiating photoreceptors displayed active Myosin caps at the apical cortex, which were not formed in cells mutant for *gek*/MRCK[25] (Fig. 2b). Loss of *gek* function also resulted in attenuation of F-actin signal at the apical membrane domain and gross defects in the morphology of the F-actin rich apical organelle known as the rhabdomere (Fig. 2c-f), which consists of a stack of approximately 60.000 microvilli, indicative of defective actomyosin contractility[22]. Introduction of a

phosphomimetic *MLC* transgene, *spaghetti squash-EE* (*sqh*^{EE}), rescued the phenotype of *gek* mutant cells, demonstrating Myosin-II activation acts downstream of *gek*/MRCK (Fig. 2g,h). MRCK is thus a conserved driver of apical Myosin activation and morphogenesis in vertebrate epithelia and *Drosophila* photoreceptors.

Apical determinant Dbl3, a Cdc42 guanine nucleotide exchange factor, controls MRCK activity

We have previously shown that the guanine nucleotide exchange factor Dbl3 activates Cdc42 at the apical pole to drive epithelial polarization and morphogenesis[17]. To determine whether Dbl3 signalling stimulates MRCK-mediated Myosin activation, we conditionally expressed Dbl3-myc in MDCK cells. This resulted in increased apical phosphorylation of MLC along with enhanced apical F-actin accumulation and microvilli induction; both inhibited by knockdown of MRCK (Fig. 3a-e). Inhibition of ROCKI/II in polarizing MDCK cells did not prevent apical actomyosin activation and morphogenesis, indicating that apical Myosin activation is not Rho dependent (Supplementary Fig. 2). Moreover, our results indicate that Dbl3 is a major activator of MRCK in mammalian cells since constitutive overexpression of MRCKβ-Flag could not rescue Db3 knockdown effects (Supplementary Fig. 3a-d). Only catalytically active, but not inactive Dbl3 that is unable to activate Cdc42[17], activated MLC phosphorylation (Fig. 3f). Thus, the activation of apical Myosin caps requires Cdc42 and MRCK activation.

To determine the temporal nature of apical MLC activation, we generated a conditional Dbl3-Myc MDCK-cell-line that constitutively expresses EGFP-MLC; the conditional Dbl3-myc transgene was then induced by the addition of tetracycline. Time-lapse fluorescence microscopy revealed that concurrent to induction of Dbl3-myc protein, increased apical EGFP-MLC activity was detected from 2.5h of tetracycline treatment (Supplementary video 1; Supplementary Fig. 3e). Analysis in fixed cells revealed that conditional expression of Dbl3-myc resulted in active Myosin cap formation 2.5 hours from the onset of tetracycline addition along with apical accumulation of MRCKβ, increasing further at 6 hours, along the expanding apical membrane domain (Fig. 4a; Supplementary Fig. 3f,g). Thus, apical MRCK recruitment and MLC phosphorylation follow the Dbl3-myc protein expression profile. Apical actomyosin cap formation correlated with apical polarization of Par6-aPKC, the brush border component Ezrin, and microvilli induction (Fig. 4a-c, Supplementary Fig. 3g). Constitutive expression of MRCKβ-flag, which is autoinhibited until bound to Cdc42-GTP, in conditional Dbl3-expressing cells accelerated the formation of apically activated Myosin caps, which became enriched with MRCKβ-flag, polarization and brush border induction (Fig. 4b,c; Supplementary Fig. 3f,g). MRCK is thus recruited to the apical membrane by Dbl3-mediated Cdc42 activation to drive apical polarization and differentiation of epithelial cells. Apical localization of MRCKβ was also observed *in vivo* in mouse renal tubules and intestine (Fig. 4d), and Gek was found at the apical photoreceptor cortex (Fig. 4e). Hence, apical MRCK polarization occurs in vitro and in vivo, and in vertebrates and invertebrates.

Apical Cdc42 activates a dual effector mechanism that antagonises junctional Myosin activity

RhoA and ROCK regulate actomyosin activity along cell-cell junctions, generating a circumferential actomyosin belt that is required for junction assembly and remodelling, and apical constriction[15, 18, 19]. Activation of apical Cdc42 by Dbl3 promotes apical expansion[17], a process opposing apical constriction. Apical Cdc42 signalling may thus not only promote apical MRCK-driven Myosin activation but also downregulate junctional actomyosin contractility to create an actomyosin activity gradient that favours apical expansion and apical PAR protein segregation. In agreement with apical activation of Myosin-II by MRCK, conditional expression of Dbl3-myc stimulated apical Cdc42 activity, as revealed by a FRET biosensor, confirming previously published loss of function experiments (Fig. 5a,b)[17]. Addition of a Cdc42 inhibitor during Dbl3 induction[26], blocked the formation of apical active Myosin caps (Fig. 5c,d). Cdc42 activation is thus required for Dbl3 to induce MRCK-dependent, apically polarized actomyosin caps. Dbl3 stimulates apical Cdc42-dependent aPKC-PAR6 effector complex activation and, hence, enrichment of aPKC at the cell cortex (Fig. 5e,f; Supplementary Fig. 4a)[17]. As aPKC is an inhibitor of the RhoA activator LULU-2[16], we asked whether Cdc42 activates a dual effector mechanism that downregulates junctional Myosin-II activity via aPKC whilst activating apical actomyosin contractility via MRCK (Fig. 5g).

To determine whether Dbl3-induced Cdc42 activation is indeed an inhibitor of RhoA at junctions, we first monitored junctional localization of LULU-2 and p114RhoGEF. The latter protein is a major junctional guanine nucleotide exchange factor for RhoA that is activated by binding to LULU-2, a FERM (4.1 protein, ezrin, radixin, moesin) domain-containing protein homologous to *Drosophila* Yurt[15, 16, 27]. Concomitant with increased aPKCζ recruitment, conditional expression of Dbl3-myc promoted LULU-2 dissociation from junctions (Fig. 6a,b; Supplementary Fig. 4d). Junctional p114RhoGEF levels also decreased upon Dbl3 induction (Fig. 6a,b; Supplementary Fig. 4d). Dbl3 induction did not affect expression levels of LULU-2 and p114RhoGEF but resulted in enhanced Ezrin phosphorylation, a marker of apical differentiation (Supplementary Fig. 4b,c). Dbl3-myc induction thus leads to reduced junctional association of proteins that activate RhoA signalling. To confirm that junctional recruitment of LULU-2 is regulated by Dbl3 activated aPKC, we knocked down Dbl3 or inhibited aPKCζ activity, which resulted in an increase in LULU-2 localization at cell junctions (Supplementary Fig. 4e-h). These results indicate that apical activation of Cdc42 antagonizes the molecular machinery that activates RhoA at cell junctions.

We next asked if RhoA activity and junctional actomyosin activation is indeed affected by Dbl3 signalling. Analysis of RhoA activity at the apical domain using a FRET biosensor revealed enriched RhoA activity at cell-cell contacts as previously reported[15]. Induction of Dbl3 expression resulted in a 50% decrease in RhoA activity at cell-cell contacts (Fig. 6c,d). Similarly, a GFP fusion protein containing the RhoA binding domain of rhotekin, another sensor to monitor the cellular distribution of active RhoA[28], was enriched at cell-cell contacts prior to Dbl3 induction but diffusely distributed when expression of the exchange factor had been induced, supporting the conclusion that enhanced Dbl3 signalling inhibits junctional

RhoA activity (Fig. 6e). Active p114RhoGEF forms a stable complex with ROCKII and Myosin-II, stimulating junctional double phosphorylation of MLC (ppMLC)[15]. Conditional expression of Dbl3 strongly reduced junctional ppMLC staining (Fig. 6f,g), further supporting an inactivation of the p114RhoGEF/RhoA pathway that promotes junctional Myosin-II activation. Thus, Dbl3 activates apical Cdc42 and thereby stimulates two effector mechanisms: induction of apical MLC phosphorylation by MRCK and aPKC-stimulated downregulation of junctional RhoA-dependent actomyosin contractility. Dbl3 signalling hence leads to a shift in the actomyosin activity gradient to stimulate apical polarization (Fig. 6h). These results further indicate distinct roles for RhoA-ROCK and Cdc42-MRCK signalling in epithelia. Indeed, loss of the RhoA effector ROCK using the null allele *rok*^{2} did not affect apical Myosin-II activation in developing pupal *Drosophila* photoreceptors (Fig. 6i), which is MRCK dependent (Fig. 2b). In contrast, adherens junction remodelling in eye imaginal discs, a *rok*-dependent process requiring junctional actomyosin activity[29], was not affected in cells mutant for *gek*/MRCK (Fig. 6k). MRCK and ROCK thus regulate distinct morphogenetic processes.

MRCK-activated Myosin-II motor activity promotes PAR protein dissociation and separation

Cortical polarization of PAR proteins is thought to rely on both biochemical signals and mechanical forces generated by actomyosin contractions[6-13]. Cdc42 activation promotes apical polarization by stimulating activation of Par6-aPKC, leading to recruitment to junctions, Par3 phosphorylation and biochemical destabilisation of the initial Par6-aPKC/Par3 complex[6, 7]. Since activation of apical actomyosin contractility by MRCK stimulates apical differentiation, we asked whether MRCK-activated Myosin-II mediates aPKC-Par6 separation from Par3 at junctions. To determine first whether MRCK activity itself is required, we used an inhibitor that blocks the catalytic activity of MRCK[30]. Induction of Dbl3-myc expression led to shift of the position of tight junctions, demarked by Par3, from the apical end of the lateral membrane towards the basal membrane, and an extended apical domain, labelled by aPKC, and a reduced basolateral domain, stained with anti-scribble antibody, as previously described (Fig. 7a)[17]. Inhibition of MRCK blocked separation of Par3 from aPKC as well as the junctional shift in control and Dbl3 overexpressing cells, indicating that MRCK activity was required even when apical Cdc42 activation and, hence, aPKC signalling[17] was increased by enhanced expression of the guanine nucleotide exchange factor. If the same experiments were repeated with blebbistatin, an inhibitor of Myosin-II motor activity that blocks actomyosin contractions[31], separation of aPKC from Par3 and junctional shifting was also inhibited, and led to increased stable complex assembly (Fig. 7b,c). Blebbistatin also strongly attenuated brush border induction (Fig. 7d,e) comparable to what we had observed in response to depletion of MRCK (Fig. 3a). Thus, these results indicate that MRCK-activated Myosin-II motor activity is required for separation of Par6-aPKC from Par3 upon apical Cdc42 activation but not for the initial recruitment of Par6-aPKC to form the tight junction-associated complex with Par3. This is in agreement with the reported diffusive properties of PAR proteins in *C. elegans,* where PAR protein segregation, but not cortical recruitment, is actomyosin-dependent[32]. Since Dbl3-mediated Cdc42 activation also stimulates aPKC to phosphorylate Par3[17] and to down-regulate junctional RhoA signalling

(Fig. 6), our results demonstrate that both effector mechanisms stimulated by active apical Cdc42 are required for apical PAR protein separation and segregation: The biochemical activity of aPKC-Par6 that destabilizes the PAR complex and downregulates junctional Myosin contractility, and the activation of apical Myosin contractility by MRCK that drives apical PAR protein separation and domain morphogenesis.

Dbl3/MRCK-stimulated actomyosin contractility drives apical segregation of PAR proteins and polarization of cytosolic brush border determinants

Cdc42-activated aPKC-Par6 recruitment to junctions is a transient process and the complex then proceeds to expand along the apical membrane, segregating from Par3 and tight junctions, to define the apical cortex[33]. Hence, we next asked whether expansion along the apical membrane is powered by MRCK-dependent and Myosin-II motor activity. Polarization of aPKC-Par6 along the apical cell cortex, which formed a stable complex, was inhibited in conditional Dbl3-myc expressing cells treated with blebbistatin and rapidly reversed following wash-out (Fig. 8a,b; Supplementary Fig. 5). The reversal of Myosin motor inhibition required MRCK kinase activity, confirming the requirement of MRCK-dependent Myosin-II activation for apical polarization of the aPKC-Par6 complex (Fig. 8c,d). It is thought that a rapid apical phosphorylation/dephosphorylation cycle of Ezrin is required to confine Ezrin and microvilli to the apical membrane domain in polarized epithelial cells, which is facilitated by apical localization of cytosolic factors such as the kinase SLK[34,35]. Similarly, NHERF-1/EBP-50 engages in a transient association with Ezrin to regulate microvillar structure[34]. Myosin motor-dependant cortical polarization was concomitant with an apical enrichment of such cytosolic regulators of brush border formation and was required for their co-localization with Ezrin at the apical pole, indicating that MRCK-induced apical domain formation included polarization of cytosolic factors required for plasma membrane specialization and morphogenesis (Fig. 8e-i and Supplementary Fig. 6). Our data thus support a model in which epithelial cortical polarization and cytosolic polarization are linked[32]. Hence, MRCK signalling unifies the mechanisms for asymmetric segregation of cytosolic components to the vicinity of the apical membrane with cortical polarization (Fig. 8j). Apical membrane staining of aPKC and Moesin in Drosophila *gek* mutant photoreceptors was also attenuated (Fig. 8k,l; Supplementary Fig. 7). These effects were rescued by co-expression of sqh^{EE}, a phosphomimetic MLC construct, in mutant *gek*/MRCK cells (Fig. 8m,n), demonstrating the importance of *gek*/MRCK activation of Myosin-II for apical differentiation of Drosophila photoreceptors.

DISCUSSION

We have identified a distinct, evolutionarily conserved actomyosin-powered morphogenetic pathway at the apical domain that is activated by Cdc42/MRCK and drives epithelial morphogenesis and the development of epithelial polarity. Cdc42/MRCK signalling serves to coordinate biochemical signalling and actomyosin-generated mechanical forces. Unlike the mechanism of action of Cdc42, the spatial activation of Cdc42 is likely to vary across species since far less GEF diversity exists in *Drosophila,* and the closest orthologue of Dbl3 in insects lacks a Sec14 domain, which is crucial for Dbl3 function in vertebrates[17].

Cell polarization is thought to be induced by mechanical forces generated by an actomyosin activity gradient[11-13, 32]. Our results indicate that apical Cdc42/MRCK signalling functions in the culminating stages of epithelial polarization leading to the accumulation of Par6 and aPKC at the apical domain by promoting the actomyosin-driven segregation of the Par6-aPKC complex from the junctional complex along the differentiating apical domain and thus promoting apical identity and morphogenesis. Moreover, cytosolic factors that regulate apical membrane specialization such as SLK and NHERF-1/EBP-50, which mediate localised Ezrin activation and brush border assembly, are concentrated at the apical pole, linking cortical and cytosolic polarization. As active Ezrin also promotes apical Dbl3 recruitment and Cdc42 activation[17], this process represents a positive feedback mechanism that enhances apical differentiation and reinforces the polarized epithelial phenotype.

Apical Cdc42 activation stimulates two cooperating effector pathways that induce the formation of apically polarized actomyosin contractility to drive PAR protein polarization: MRCK-mediated apical Myosin-II activation and Par6-aPKC-mediated inhibition of junctional RhoA activation via negative regulation of LULU-2 and p114RhoGEF and, hence, reduced junctional actomyosin contractility. The biochemical activity of aPKC-Par6 also supports apical PAR segregation by phosphorylating Par3 and, thereby, destabilising its interaction with the aPKC-Par6 complex[6, 7, 17]. Hence, activation of the two Cdc42 effector pathways integrates biochemical and mechanical force-generating pathways stimulating apical segregation of PAR proteins, polarization and domain morphogenesis. The downregulation of junctional RhoA signalling by apical Cdc42 activation further suggests a sequential model for the function of ROCK and MRCK in Myosin-II activation: RhoA/ROCK signalling drives early steps of junction formation[15] and remodelling such as in the early eye disc[29, 36, 37], subsequent Cdc42/MRCK activation then leads to a reorientation of the actomyosin contractility gradient and, hence, apical polarization and differentiation. The antagonism between junctional RhoA and apical Cdc42 signalling may be bidirectional. In vertebrates, junctional RhoA activity is generated by p114RhoGEF, a pathway that is stimulated in cells that undergo apical constriction due to increased levels of LULU-2[15, 16]. The fly homologue of LULU-2, Yurt, regulates apical domain size negatively by inhibiting the activity of Crumbs, which is positively regulated by aPKC[27], suggesting that LULU-2/Yurt signalling may indeed antagonize apical Cdc42-driven mechanisms. Hence, mechanisms of mutual antagonism between Cdc42/MRCK and RhoA/ROCK driven actomyosin contractility may exist that create a cellular code for dynamic polarized morphogenetic processes underlying the generation of tissue- and organ-specific cell surface fates during differentiation of various cell types.

METHODS

Methods, including statements of data availability and references, are available in the online version of this paper.

ACKNOWLEDGEMENTS

This work was supported by the BBSRC (BB/L007584/1 and BB/N014855/1) and the Wellcome Trust (099173/Z/12/Z). Work in FP lab, including support to EV, was funded by an MRC grant (MC-

_UU_12018/3). The N2 A71 monoclonal antibodies, developed by Eric Wieschaus was obtained from the Developmental Studies Hybridoma Bank, created by the NICHD of the NIH and maintained at The University of Iowa, Department of Biology, Iowa City, IA 52242. Stocks obtained from the Bloomington Drosophila Stock Center (NIH P40OD018537) were used in this study.

AUTHOR CONTRIBUTIONS

CZ performed most of the vertebrate and EV the *Drosophila* experiments. All other authors performed particular subsets of experiments. CZ, MSB and KM designed the project and drafted the manuscript. All authors read and contributed to the final version of the manuscript.

COMPETING INTERESTS

The authors declare that they have no competing financial interests.

REFERENCES

1. Mellman, I. & Nelson, W.J. Coordinated protein sorting, targeting and distribution in polarized cells. *Nat Rev Mol Cell Biol* **9**, 833-845 (2008).
2. Sauvanet, C., Wayt, J., Pelaseyed, T. & Bretscher, A. Structure, regulation, and functional diversity of microvilli on the apical domain of epithelial cells. *Annu Rev Cell Dev Biol* **31**, 593-621 (2015).
3. Zihni, C., Mills, C., Matter, K. & Balda, M.S. Tight junctions: from simple barriers to multifunctional molecular gates. *Nat Rev Mol Cell Biol* **17**, 564-580 (2016).
4. Cowan, C.R. & Hyman, A.A. Acto-myosin reorganization and PAR polarity in C. elegans. *Development* **134**, 1035-1043 (2007).
5. St Johnston, D. & Ahringer, J. Cell polarity in eggs and epithelia: parallels and diversity. *Cell* **141**, 757-774 (2010).
6. Morais-de-Sa, E., Mirouse, V. & St Johnston, D. aPKC phosphorylation of Bazooka defines the apical/lateral border in Drosophila epithelial cells. *Cell* **141**, 509-523 (2010).
7. Walther, R.F. & Pichaud, F. Crumbs/DaPKC-dependent apical exclusion of Bazooka promotes photoreceptor polarity remodeling. *Curr Biol* **20**, 1065-1074 (2010).
8. Hird, S.N. & White, J.G. Cortical and cytoplasmic flow polarity in early embryonic cells of Caenorhabditis elegans. *J Cell Biol* **121**, 1343-1355 (1993).
9. Cheeks, R.J. *et al.* C. elegans PAR proteins function by mobilizing and stabilizing asymmetrically localized protein complexes. *Curr Biol* **14**, 851-862 (2004).
10. Munro, E., Nance, J. & Priess, J.R. Cortical flows powered by asymmetrical contraction transport PAR proteins to establish and maintain anterior-posterior polarity in the early C. elegans embryo. *Dev Cell* **7**, 413-424 (2004).
11. Mayer, M., Depken, M., Bois, J.S., Julicher, F. & Grill, S.W. Anisotropies in cortical tension reveal the physical basis of polarizing cortical flows. *Nature* **467**, 617-621 (2010).
12. Bois, J.S., Julicher, F. & Grill, S.W. Pattern formation in active fluids. *Phys Rev Lett* **106**, 028103 (2011).
13. Goehring, N.W. *et al.* Polarization of PAR proteins by advective triggering of a pattern-forming system. *Science* **334**, 1137-1141 (2011).
14. Lecuit, T. & Lenne, P.F. Cell surface mechanics and the control of cell shape, tissue patterns and morphogenesis. *Nat Rev Mol Cell Biol* **8**, 633-644 (2007).
15. Terry, S.J. *et al.* Spatially restricted activation of RhoA signalling at epithelial junctions by p114RhoGEF drives junction formation and morphogenesis. *Nat Cell Biol* **13**, 159-166 (2011).
16. Nakajima, H. & Tanoue, T. Lulu2 regulates the circumferential actomyosin tensile system in epithelial cells through p114RhoGEF. *J Cell Biol* **195**, 245-261 (2011).
17. Zihni, C. *et al.* Dbl3 drives Cdc42 signaling at the apical margin to regulate junction position and apical differentiation. *J Cell Biol* **204**, 111-127 (2014).
18. Mooseker, M.S. Organization, chemistry, and assembly of the cytoskeletal apparatus of the intestinal brush border. *Annu Rev Cell Biol* **1**, 209-241 (1985).
19. Castillo, A.M., Lagunes, R., Urban, M., Frixione, E. & Meza, I. Myosin II-actin interaction in MDCK cells: role in cell shape changes in response to Ca2+ variations. *J Muscle Res Cell Motil* **19**, 557-574 (1998).
20. St Johnston, D. & Sanson, B. Epithelial polarity and morphogenesis. *Curr Opin Cell Biol* **23**, 540-546 (2011).
21. Unbekandt, M. & Olson, M.F. The actin-myosin regulatory MRCK kinases: regulation, biological functions and associations with human cancer. *J Mol Med (Berl)* **92**, 217-225 (2014).
22. Reifegerste, R. & Moses, K. Genetics of epithelial polarity and pattern in the Drosophila retina. *Bioessays* **21**, 275-285 (1999).
23. Pocha, S.M. & Knust, E. Complexities of Crumbs function and regulation in tissue morphogenesis. *Curr Biol* **23**, R289-293 (2013).

24. Walther, R.F., Nunes de Almeida, F., Vlassaks, E., Burden, J.J. & Pichaud, F. Pak4 Is Required during Epithelial Polarity Remodeling through Regulating AJ Stability and Bazooka Retention at the ZA. *Cell Rep* **15**, 45-53 (2016).
25. Gontang, A.C., Hwa, J.J., Mast, J.D., Schwabe, T. & Clandinin, T.R. The cytoskeletal regulator Genghis khan is required for columnar target specificity in the Drosophila visual system. *Development* **138**, 4899-4909 (2011).
26. Hong, L. *et al.* Characterization of a Cdc42 protein inhibitor and its use as a molecular probe. *J Biol Chem* **288**, 8531-8543 (2013).
27. Laprise, P. *et al.* Yurt, Coracle, Neurexin IV and the Na(+),K(+)-ATPase form a novel group of epithelial polarity proteins. *Nature* **459**, 1141-1145 (2009).
28. Benink, H.A. & Bement, W.M. Concentric zones of active RhoA and Cdc42 around single cell wounds. *J Cell Biol* **168**, 429-439 (2005).
29. Robertson, F., Pinal, N., Fichelson, P. & Pichaud, F. Atonal and EGFR signalling orchestrate rok- and Drak-dependent adherens junction remodelling during ommatidia morphogenesis. *Development* **139**, 3432-3441 (2012).
30. Unbekandt, M. *et al.* A novel small-molecule MRCK inhibitor blocks cancer cell invasion. *Cell Commun Signal* **12**, 54 (2014).
31. Bond, L.M., Tumbarello, D.A., Kendrick-Jones, J. & Buss, F. Small-molecule inhibitors of myosin proteins. *Future Med Chem* **5**, 41-52 (2013).
32. Hoege, C. & Hyman, A.A. Principles of PAR polarity in Caenorhabditis elegans embryos. *Nat Rev Mol Cell Biol* **14**, 315-322 (2013).
33. Zihni, C., Balda, M.S. & Matter, K. Signalling at tight junctions during epithelial differentiation and microbial pathogenesis. *J Cell Sci* **127**, 3401-3413 (2014).
34. Viswanatha, R., Bretscher, A. & Garbett, D. Dynamics of ezrin and EBP50 in regulating microvilli on the apical aspect of epithelial cells. *Biochem Soc Trans* **42**, 189-194 (2014).
35. Viswanatha, R., Ohouo, P.Y., Smolka, M.B. & Bretscher, A. Local phosphocycling mediated by LOK/SLK restricts ezrin function to the apical aspect of epithelial cells. *J Cell Biol* **199**, 969-984 (2012).
36. Escudero, L.M., Bischoff, M. & Freeman, M. Myosin II regulates complex cellular arrangement and epithelial architecture in Drosophila. *Dev Cell* **13**, 717-729 (2007).
37. Corrigall, D., Walther, R.F., Rodriguez, L., Fichelson, P. & Pichaud, F. Hedgehog signaling is a principal inducer of Myosin-II-driven cell ingression in Drosophila epithelia. *Dev Cell* **13**, 730-742 (2007).

Figure 1

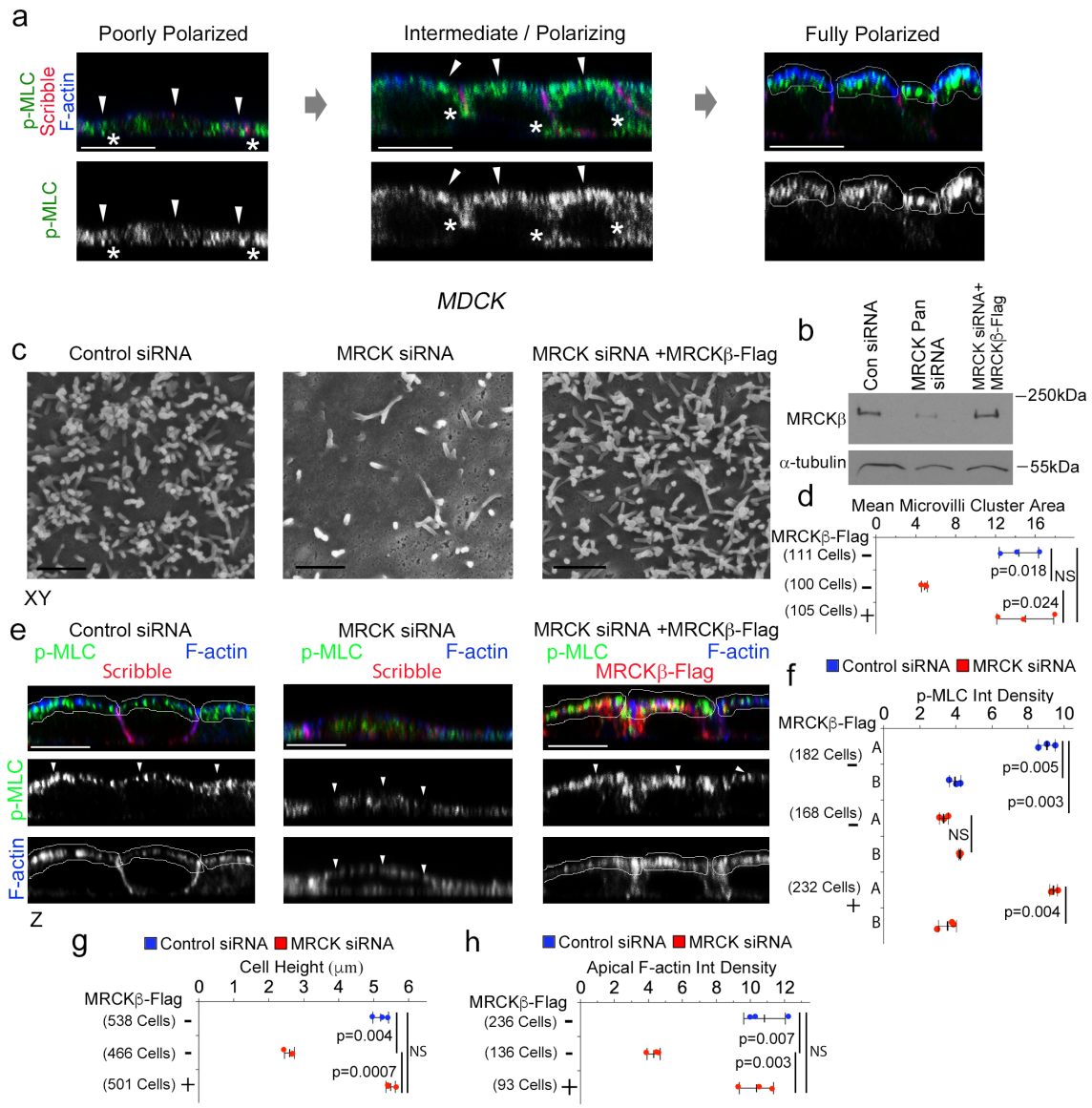

Figure 1: MRCK activates apical actomyosin contractility that controls apical morphogenesis. (**a**) Spontaneous polarization of MDCK cells leads to the formation of apical actomyosin caps positive for p-MLC and F-actin. (**b**) Expression of MRCKβ as analysed by immunoblotting of total cell extracts. (**c,d**) Scanning electron microscopy of apical domains reveals levels of microvilli induction by MDCK cells upon depletion of MRCK without or with complementation with exogenously expressed MRCKβ-flag. (**e,f**) Measurement of active Myosin at cortical caps (A) and basal membrane (B) during polarization and differentiation of cells depleted of or rescued for MRCK expression by confocal immunofluorescence microscopy. (**g,h**) Measured cell height and F-actin levels in polarizing cells with or without MRCK function. For all quantifications, n=3 independent experiments and shown are the data points, means ± 1 SD (in black), the total number of cells analysed for each type of sample across all experiments, and p-values derived from t-tests. Arrowheads point to the apical cortex demarked by F-actin. Unprocessed original scans of blots are shown in Supplementary Figure 8. Scale bars: electron micrographs, 1μm; confocal immunofluorescence images, 10μm.

Figure 2

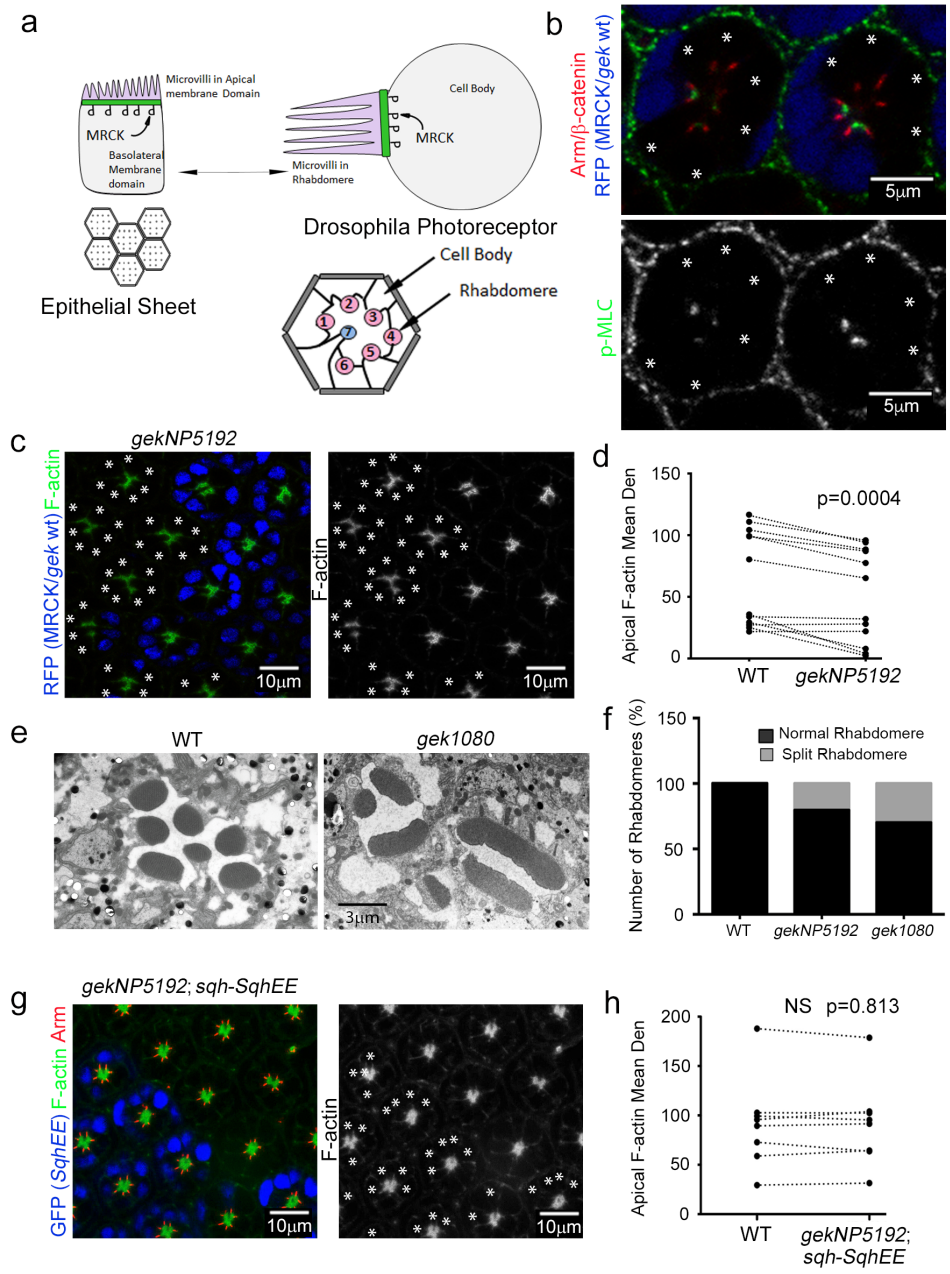

Figure 2: MRCK/*gek* regulates apical Myosin activation and morphogenesis in differentiating Drosophila photoreceptors. (**a**) Scheme illustrating the similarities and corresponding plasma membrane domains of vertebrate epithelial cells and *Drosophila* photoreceptors. Indicated are apical microvilli and the apical zone enriched in active Myosin-II. (**b-d**) Confocal sections of *Drosophila* pupal mosaic retinas showing wild type cells (blue nuclei) and cells mutant for *gek* were stained for F-actin (c) or p-MLC (b). Mutant cells are labelled with asterisks. Quantification of apical actin enrichment shows analysis of wild type and mutant cells (paired within sections; n represents 11 animals, a t-test was used to calculate the p value). (**e,f**) Analysis of rhabdomere integrity in wild type and *gek* mutant cells using 2 different *gek* alleles (gek^{NP5192} or gek^{1080}) demonstrates severe defects including splitting. (**g,h**) Confocal sections of *Drosophila* eyes showing wild type cells and cells mutant for gek^{NP5192} but expressing $sqh\text{-}Sqh^{EE}$ (blue nuclei; labelled with asterisks; the quantification represents pairs within sections and is based on n = 8 animals, a t-test was used to calculate the p value).

Figure 3

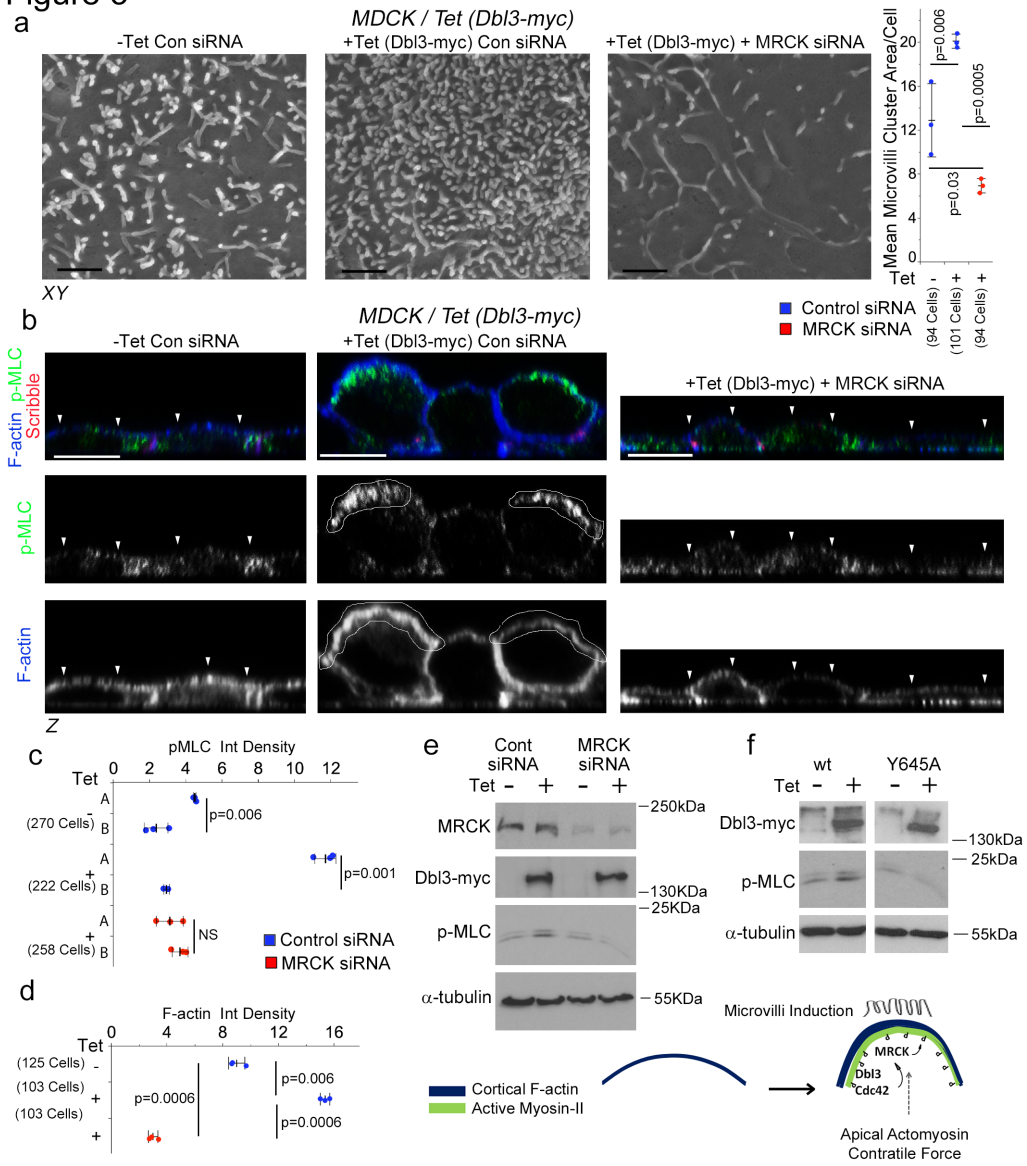

Figure 3: MRCK functions as an effector of Dbl3-Cdc42 signalling. (**a**) Scanning electron microscopy analysis of microvilli induction by MDCK cells with tetracycline-inducible Dbl3-myc expression transfected with MRCK siRNA determined by measuring areas of microvilli clusters from SEM scans. (**b-d**) Induction of active Myosin at cortical caps (A) or basal membrane (B), and enrichment of F-actin at the apical cortex during polarization and differentiation, stimulated by conditional expression of Dbl3-myc with or without MRCK siRNA knockdown. White arrowheads highlight the apical membrane cortex labelled for F-actin. (**e**) Immunoblot analysis of total active Myosin levels following conditional expression of Dbl3-myc and siRNA knockdown of MRCK. (**f**) Immunoblot analysis of total active Myosin-II levels following conditional expression of Dbl3-myc or GEF inactive Dbl3Y645A-myc. The schematic illustrates the formation of apical caps formed by activated Myosin-II and F-actin. Unprocessed original scans of blots are shown in Supplementary Figure 8. For all quantifications, n=3 independent experiments and shown are the data points, means ± 1 SD (in black), the total number of cells analysed for each type of sample across all experiments, and p-values derived from t-tests. Scale bars: a, 1µm; b, 10µm.

Figure 4

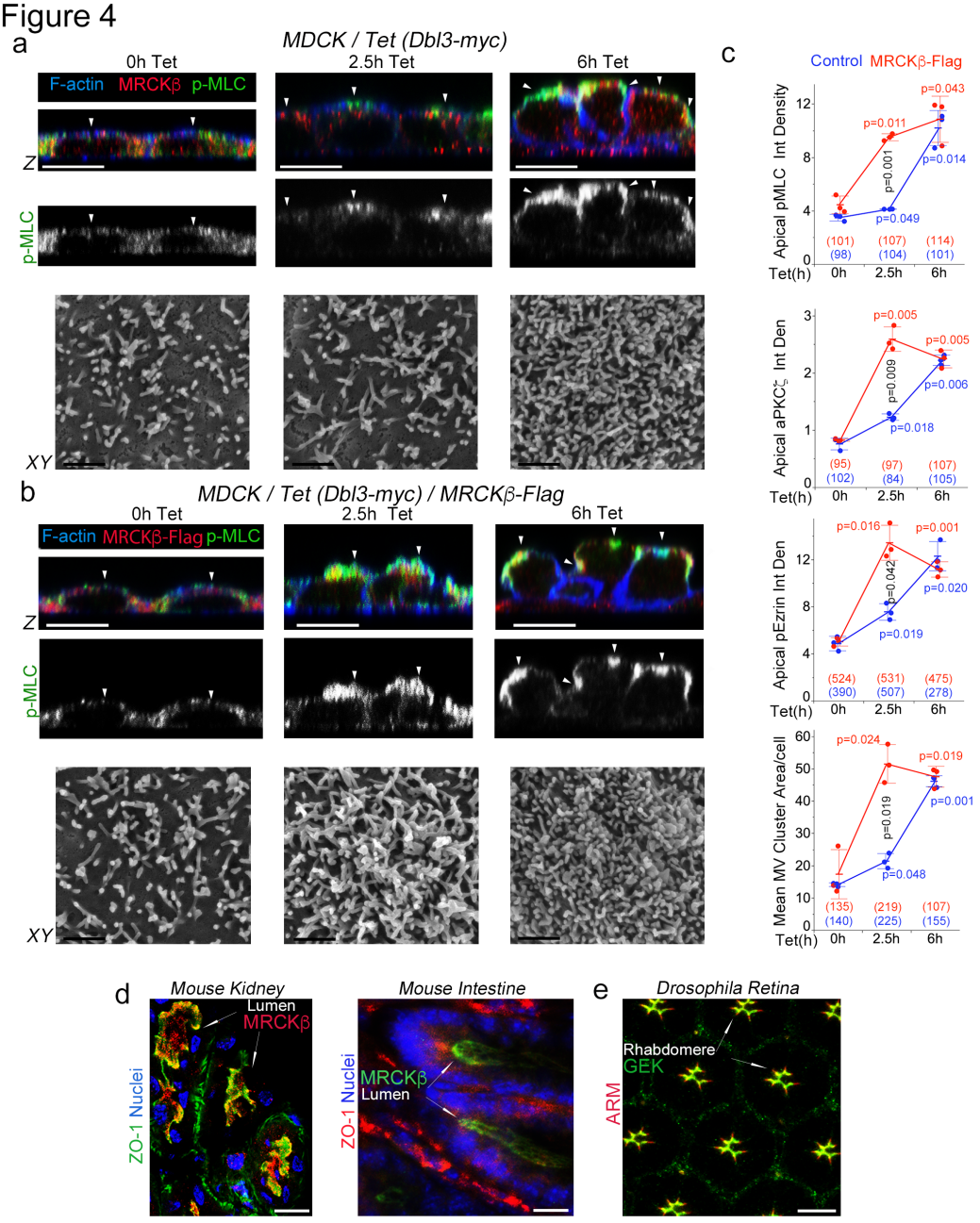

Figure 4: Cdc42 activates MRCK apically, stimulating apical Myosin-II activation and differentiation. (**a-c**) Analysis and quantification of apical pMLC, aPKCζ and pEzrinT567 at the apical membrane domain using confocal z-section analysis and of brush border induction using scanning electron microscopy of MDCK cells with tetracycline-inducible Dbl3-myc expression with or without constitutive expression of MRCKβ-flag. White arrowheads highlight the apical membrane cortex labelled for F-actin. (**d**) Localization of MRCKβ in mouse kidney and small intestine. (**e**) Localization of Gek in polarizing pupal *Drosophila* photoreceptors. For all quantifications, n=3 independent experiments and shown are the data points, means ± 1 SD, the total number of cells analysed for each type of sample across all experiments, and p-values derived from t-tests (red/blue values refer to comparisons within categories and black value to comparisons between categories after 2.5h). In panels **d** and **e**, arrows point to apical domains positive for MRCK/Gek. Scale bars: electron micrographs, 1µm; confocal immunofluorescence images, 10 µm.

Figure 5

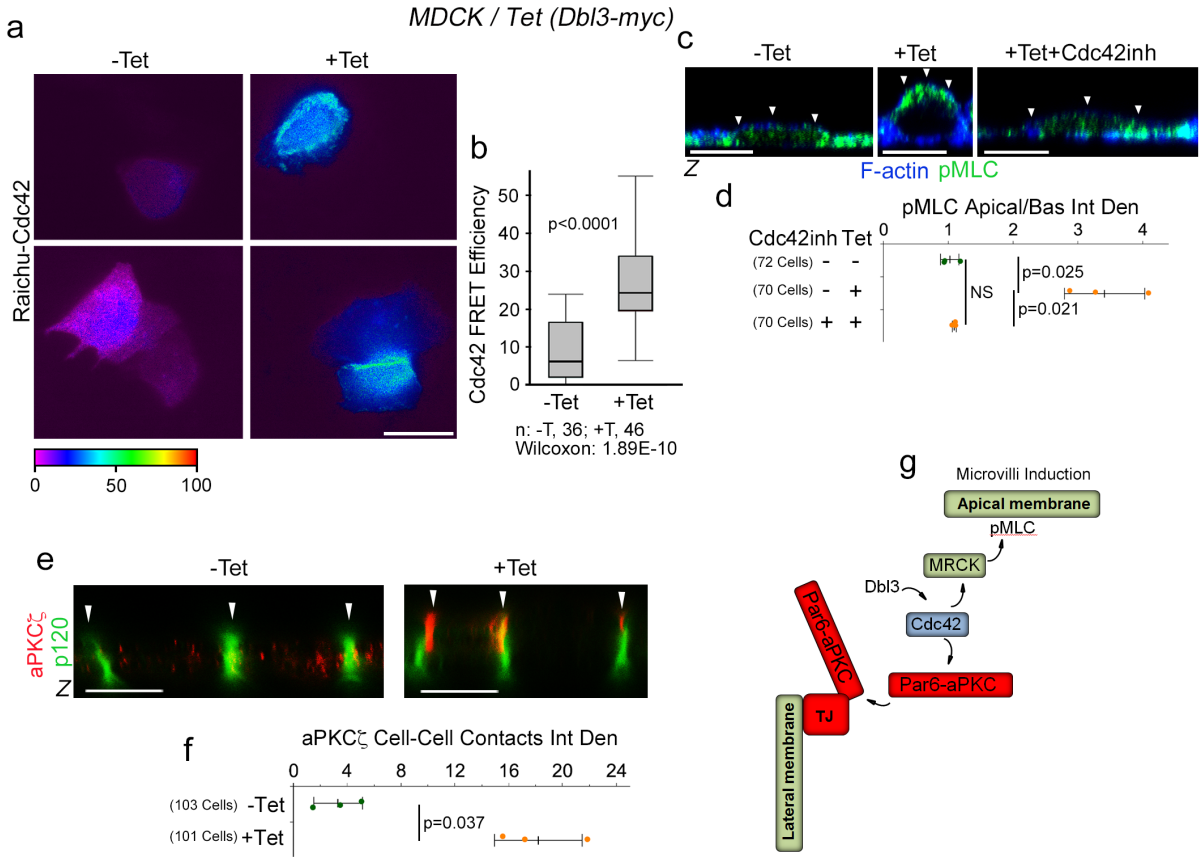

Figure 5: Dbl3 and Cdc42 drive apical actomyosin activation and aPKC recruitment. (**a,b**) FRET analysis of Cdc42 activity at the apical aspect of MDCK cells conditionally expressing Dbl3-myc. (**c,d**) Confocal microscopy of pMLC and F-actin at the apical membrane domain of MDCK cells conditionally expressing Dbl3-myc induced with tetracycline in the absence or presence of Cdc42 inhibitor. White arrowheads highlight the apical membrane cortex labelled for F-actin. (**e,f**) Analysis of aPKCζ localization in MDCK cells with tetracycline-inducible Dbl3-myc expression. White arrowheads point to the lateral junctional complex. (**g**) Schematic diagram illustrating activation of two effector mechanisms, MRCK/Myosin-II and Par6-aPKC by Dbl3 stimulated apical Cd42-activation. Quantifications show shown are (b) box blots (25th to 75th percentiles, with a line at the median; whiskers extend to the max/min data points; n=36 cells -Tet and n=46 cells +Tet; p value was calculated with a Wilcoxon test), or (d, f) based on n=3 independent experiments and showing the data points, means ± 1 SD (in black), the total number of cells analysed for each type of sample across all experiments, and p-values derived from t-tests. Scale bars: 10 μm.

Figure 6

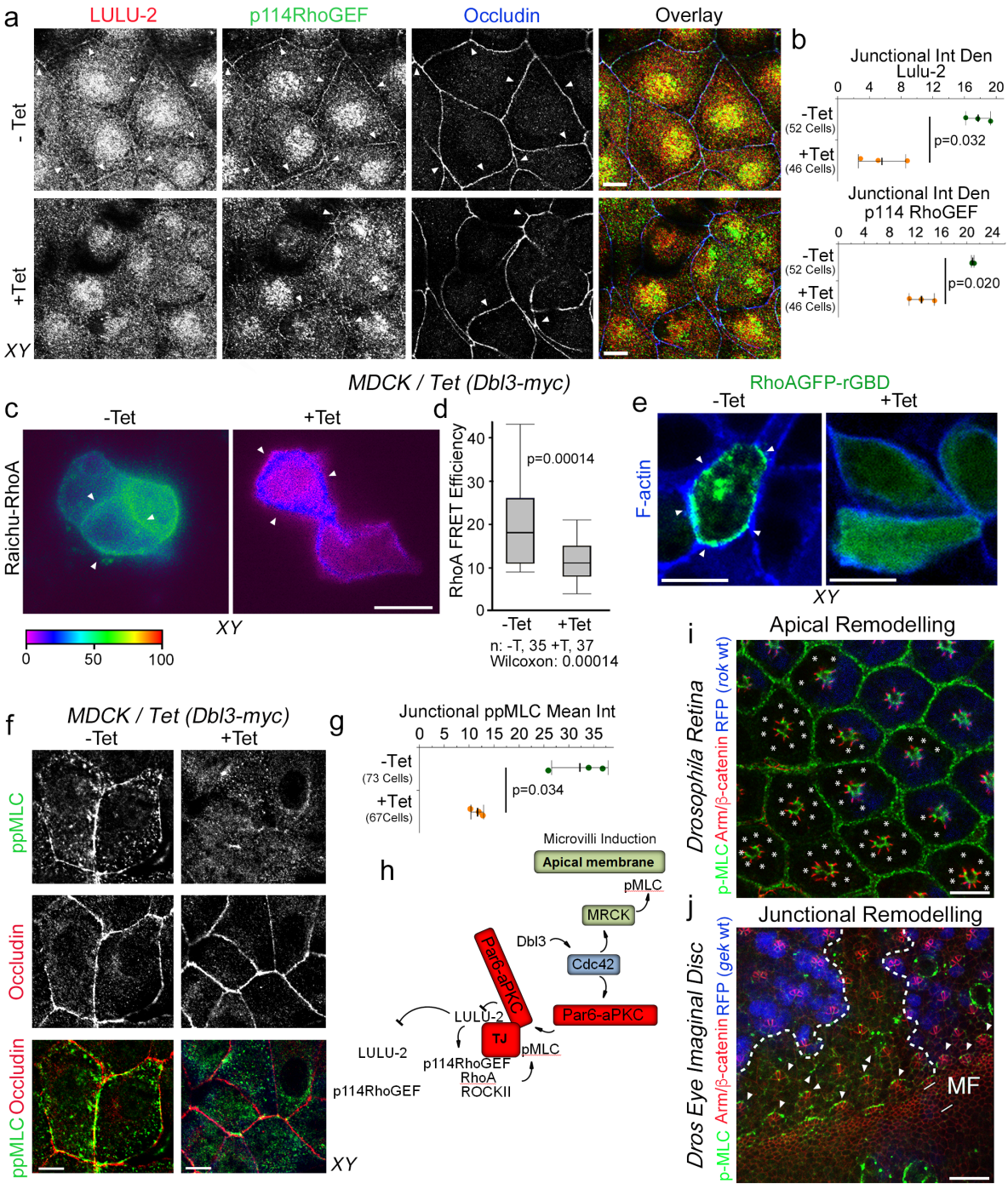

Figure 6: Apical activation of Cdc42 by Dbl3 antagonizes junctional RhoA-stimulated Myosin-II activation. (**a,b**) Conditional tetracycline-induced expression of Dbl3 in MDCK cells stimulates loss of junctional RhoA signalling components p114RhoGEF and LULU-2. Shown are confocal xy and z-sections. Junctions are indicated by white arrowheads. (**c,d**) FRET analysis of RhoA activity in MDCK cells conditionally expressing Dbl3-myc (white arrowheads indicate cell-cell contacts) (**e**) Confocal analysis of MDCK cells transiently expressing the active RhoA binding domain of rhotekin fused to GFP (GFP-rGBD), conditionally expressing Dbl3-myc (white arrowheads indicate cell-cell junctions). (**f,g**) Confocal analysis of junctional pMLC activity in MDCK cells conditionally expressing Dbl3-myc. (**i**) Confocal sections of a *Drosophila* retina showing wild type cells (blue) and

cells mutant for the RhoA effector null allele *rok*^{2} (white asterisks) that were stained for pMLC and Armadillo (Arm), the orthologue of mammalian β-catenin. White asterisks indicate *rok*^{2}-mtant cells. (**j**) Maximum intensity projection of confocal sections of a mosaic *Drosophila* eye imaginal disc showing wild type cells (blue nuclei) and cells mutant for *gek*^{NP5192} and stained for Armadillo (Arm) and pMLC (MF, morphogenetic furrow; the dashed white lines indicate the borders between wild type and mutant cells; arrowheads point to Myosin-II-rich cell junctions). The schematic diagram illustrates the generation of apically polarized actomyosin activation by apical activation of MRCK and inactivation of junctional RhoA signalling by aPKC. Quantifications show shown are (d) box blots (25th to 75th percentiles, with a line at the median; whiskers extend to the max/min data points; n=35 cells -Tet and n=37 cells +Tet; p value was calculated with a Wilcoxon test), or (b, d, g) based on n=3 independent experiments and showing the data points, means ± 1 SD (in black), the total number of cells analysed for each type of sample across all experiments, and p-values derived from t-tests. Scale bars: 10 μm.

Figure 7

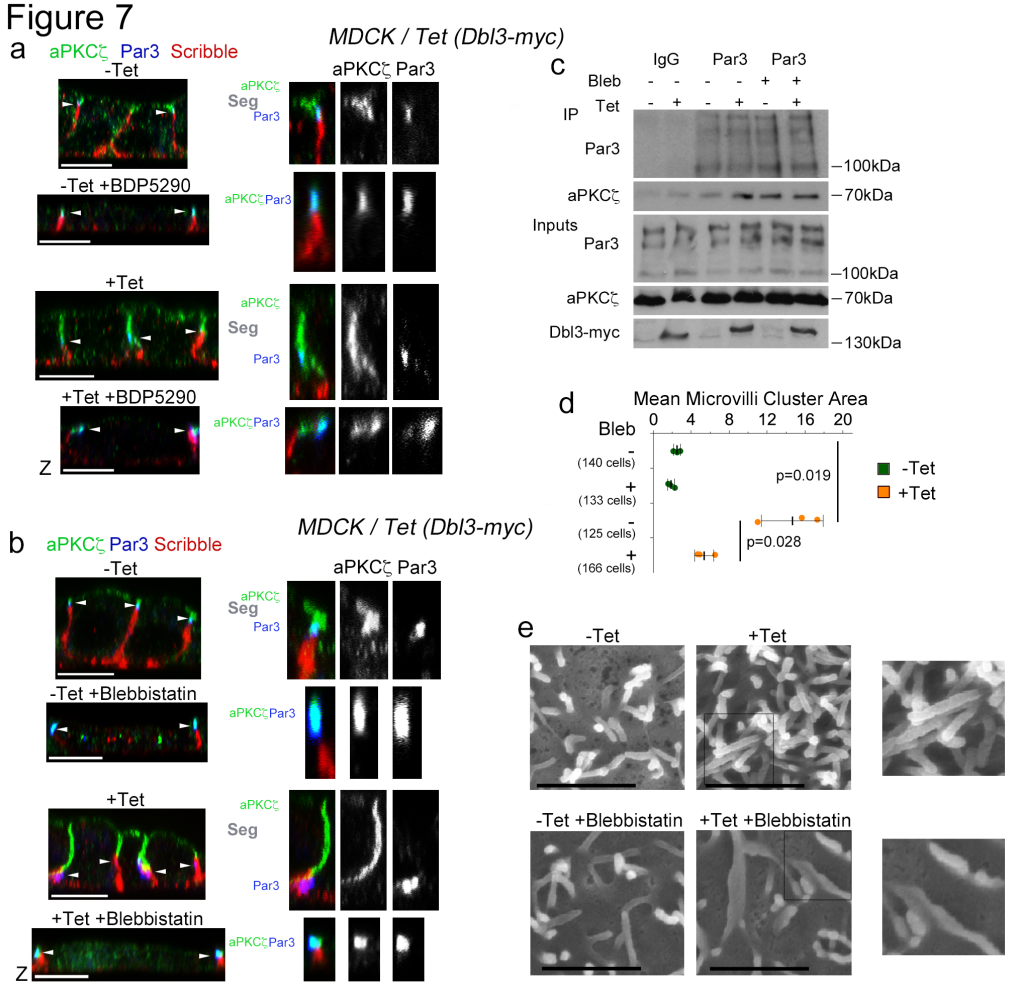

Figure 7: MRCK-stimulated Myosin-II activation drives PAR separation at tight junctions. (**a,b**) Confocal analysis of aPKCζ localization at tights junctions in medium/advanced polarizing/differentiating MDCK cells with tetracycline-inducible Dbl3-myc expression without or with (**a**) BDP5290, a MRCK inhibitor, or (**b**) blebbistatin, a Myosin-II inhibitor. The position of tight junctions, demarked by Par3, is indicated by white arrowheads. Note, tight junctions move towards the basal membrane in response to apical expansion[17]. The larger magnifications show examples of cells in which aPKC segregates from Par3 (all controls and enhanced by Dbl3-myc expression) or in which aPKC and Par3 co-localise (cells treated with MRCK or Myosin-II inhibitor). aPKCζ segregation from Par3 at tight junctions is highlighted by 'Seg'. (**c**) Immunoprecipitation analysis of aPKCζ-Par3 complex formation in cells conditionally expressing Dbl3-myc with or without blebbistatin. Note, increased Par3-aPKC complex formation in Dbl3-myc-induced cells without blebbistatin is due to increased transient interactions that promote apical expansion[17]. (**d,e**) Quantification of microvilli induction in MDCK cells conditionally expressing Dbl3-myc -/+ Myosin-II inhibition. The quantification in panel d is based on n=3 independent experiments and shown are the data points, means ± 1 SD (in black), the total number of cells analysed for each type of sample across all experiments, and p-values derived from t-tests. Unprocessed original scans of blots are shown in Supplementary Figure 8. Scale bars: electron micrographs, 1µm; confocal immunofluorescence images, 10 µm.

Figure 8

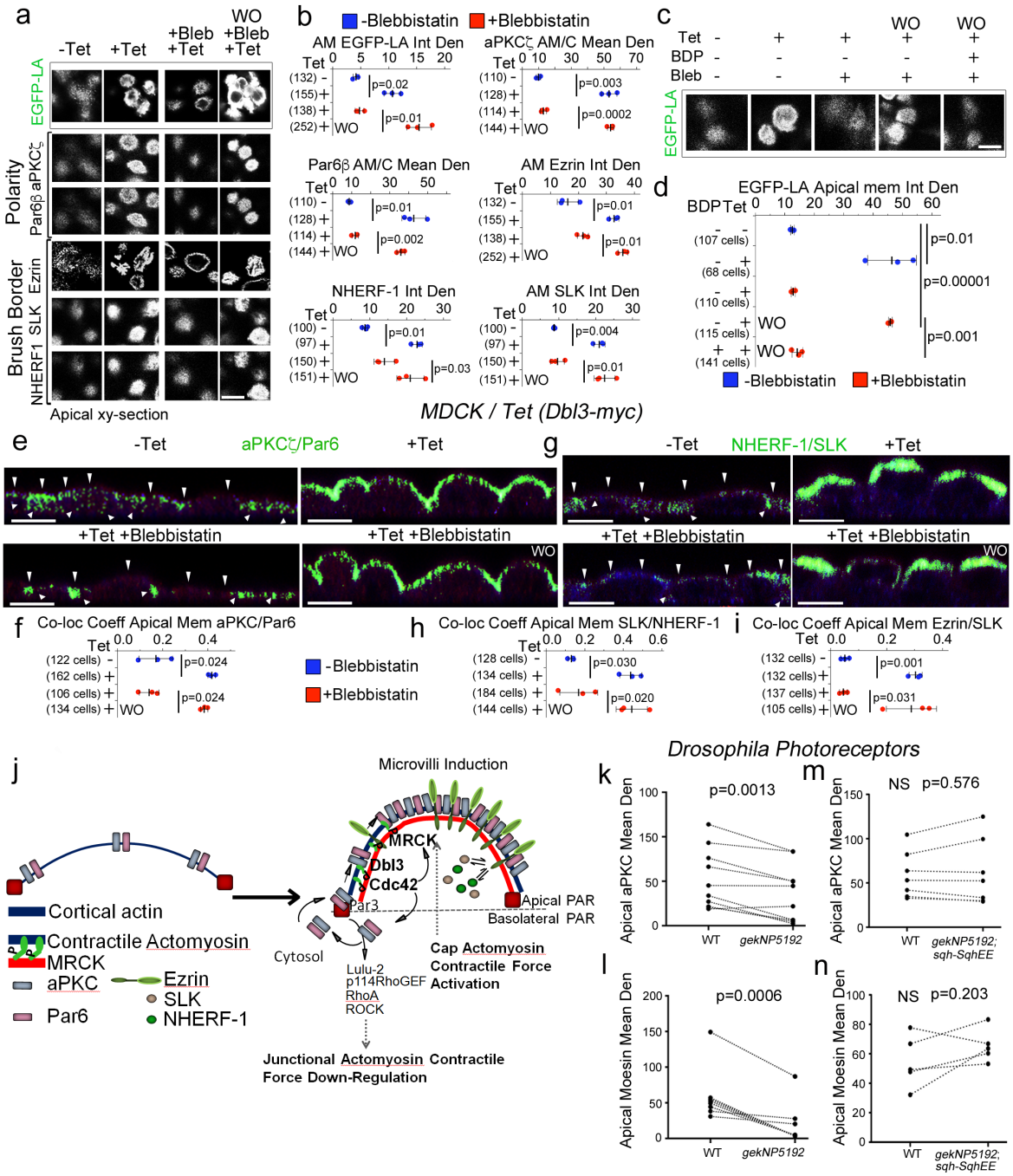

Figure 8: MRCK-activated actomyosin contractility drives apical PAR segregation and polarization of cytosolic factors. (**a,b**) Levels of EGFP-Lifeact (EGFP-LA), Par polarity and brush border proteins localized at the apical membrane domain in MDCK cells conditionally expressing Dbl3-myc, treated with blebbistatin and followed by washout (WO). (**c,d**) Levels of EGFP-Lifeact (EGFP-LA) enrichment at the apical membrane domain of MDCK cells conditionally expressing Dbl3-myc following blebbistatin treatment and washout in the absence or presence of BDP5290 to inhibit catalytic activity of MRCK. (**e-i**) Measurements of co-localization coefficients of PAR polarity and brush border proteins at the apical membrane domain in MDCK cells conditionally expressing Dbl3-myc transiently inhibited with blebbistatin followed by wash out for 2 hours (green indicates co-localisation, see also Supplementary figures 5 and 6; arrowheads point to apical membrane). (**j**) Schematic model

of polarity induced by apical stimulation of Cdc42, activating a dual effector mechanism to generate asymmetric actomyosin contractions, apical PAR domain formation and membrane morphogenesis. Bright green represents co-localization of Par and brush border proteins. (**k-n**) Quantification of confocal sections of pupal retinas stained for the apical markers aPKC and Moesin comparing wild type cells and *gek* mutant cells (**k, l**), or wild type cells and cells mutant for *gek* expressing Sqh^{EE} (**m, n**). Quantifications in panels b, d, f, h, and i are based on n=3 independent experiments and shown are the data points, means ± 1 SD (in black), the total number of cells analysed for each type of sample across all experiments, and p-values derived from t-tests. Quantifications in panels k-n of protein expression levels compare measurements from wild type and neighbouring mutant cells (paired within sections; see Supplementary Fig. 7 for representative images); k, n=10 animals; l, n=8 animals; m and n, n=7 animals; p values were calculated with t-tests). Scale bars: 10 µm.

METHODS

Cell culture and generation of mammalian expression vectors and cell Lines

MDCK and Caco-2 cells were grown in DMEM supplemented with 10% or 20%, respectively, foetal bovine serum (original cell stocks were obtained from Ira Mellman (MDCK cells) and Hans-Peter Hauri (Caco-2 cells) [17, 38, 39]. Fresh batches of cells from a contamination-free stock that had been tested for mycoplasma (MycoAlert; Promega Inc.) were used to replace fresh cultures every 6 to 8 weeks. Cells were then weekly stained with Hoechst dye to reveal nuclei and DNA of contaminants such as mycoplasma. MRCK inhibitor BDP5290 was synthesized by the Cancer Research UK Beatson Institute Drug Discovery Group and used at a concentration of 10μM. Blebbistatin (10μM final concentration), the Cdc42 inhibitor ML141 (10μM), and the ROCKI/II inhibitor GSK 269962 (10nM) were purchased from Tocris Bioscience. The aPKCζ-myristoylated inhibitor was purchased from Merck Millipore and used at a concentration of 40μM. For conditional expression of Dbl3-myc, Dbl3 pcDNATO-myc expression vector system was constructed as described in Zihni et al., 2014[17]. MDCK cells were transfected with a plasmid encoding the tetracycline repressor (pcDNA6-TR) using the calcium phosphate method[17], cultured in DMEM with 10% foetal bovine serum and selected with Blasticidin (0.5μg/ml). Selected clones were then transfected with pCDNA4TO-Dbl3-myc and selected in DMEM with 10% foetal bovine serum with Blasticidin (0.5μg/ml; PAA Laboratories Inc.) and Zeocin (200μg/ml; Thermo Fisher Scientific). The MDCK pcDNA4TO-Dbl3-myc/MRCKβ-flag cell-line was generated by transfecting rat MRCKβ-flag into the MDCK pcDNATO-Dbl3-myc TET-R cell-line and selecting in DMEM with 10% foetal bovine serum with Blastocidin (0.5μg/ml), Zeocin (200μg/ml) and G418/Geneticin (600μg/ml; Thermo Fisher Scientific). MDCK and Caco-2 cells constitutively expressing MRCKβ-flag were transfected analogously and cultured in DMEM with either 10% or 20% foetal bovine serum and G418 (600μg/ml G418). To generate EGFP-LA or EGFP-MLC pcDNA4TO-Dbl3-myc MDCK TET-R cell-lines retroviral transduction constructs EGFP-Lifeact were cloned at EcoRI and XhoI sites using the following primers: 5' GAA TTC ATG GGT GTC GCA GAT TTG ATC AAG AAA TTC GAA AGC ATC TCA AAG GAA GAA CTC GAG 3' and 5' CTC GAG TTC TTC CTT TGA GAT GCT TTC GAA TTT CTT GAT CAA ATC TGC GAC ACC CAT GAA TTC 3' and MLC by PCR amplification using the following primers 5' CAA TAA GAA TTC ATG TCC AGC AAG CGG GCC AAA GC 3' and 5' GAC TTC CTC GAG CTA GTC GTC TTT ATC CTT GGC G 3' into retroviral packing vector pMSC28 EGFP IRES Puro, a MLV-based retroviral system as described previously[40]. Constructs were co-transfected with pVSVG into GP2-293 cells (Clontech). Supernatants were collected, clarified by centrifugation (200XG, 5 mins) filtered (0.45μm) and used to infect MDCK Dbl3 Tet-R cells in the presence of 8μg/ml polybrene (Millipore) at (MOI) <1. Cell lines were selected for with either Puromycin or G418 (Thermo Fisher Scientific) at final concentration of 2.0μg/ml or 800μg/ml respectively. Selected clonal cell lines were grown on maintenance concentration of 0.5μg/ml Puromycin or 400μg/ml G418.

Transfection

Cells were cultured and transfected using Interferin transfection reagent (Polyplus Transfection) using the method described in Zihni et al.[17] using siRNAs targeting the following sequences: human MRCKpan 5'-CGAGAAGACTTTGAAATAA-3'; canine MRCKpan 5'-AGAGAAGACTTTGAGATAT-3'; canine Dbl3 5'-AAGAUAUCGCCUUCUUGUC-3'. The MRCK siRNA sequences are not conserved in the rat mRNA, enabling rescue experiments with the rat cDNA encoding MRCKβ.

Mammalian antibodies and immunological methods

Fixation and processing cells and mouse tissue sections was as previously described[19]. The following antibodies were used: EHM2/Lulu-2, goat polyclonal (abcam ab77484) 1/50 for immunofluorescence and 1/250 for immunoblotting[16]; Par3, rabbit polyclonal (Upstate, Millipore 07-330) 1/500 for immunofluorescence and 1/2000 for immunoblotting; PAR6β, rabbit polyclonal H-64 (Santa Cruz Biotechnology sc-67392) 1/200 for immunofluorescence and 1/1000 for immunoblotting; aPKCζ, mouse monoclonal (Santa Cruz Biotechnology sc-17781) 1/200 for immunofluorescence and 1/1000 for immunoblotting; occludin, mouse monoclonal (Invitrogen, ThermoFisher Scientific 33-150) 1/1000 for immunofluorescence; Scribble, goat polyclonal (Santa Cruz Biotechnology sc-11049) immunofluorescence 1/200; MRCKβ, rabbit polyclonal (Santa Cruz Biotechnology sc-48834) immunofluorescence 1/200 and immunoblotting 1/500, Ezrin Mouse monoclonal 3C12 (Santa Cruz Biotechnology sc-58758) immunofluorescence 1/500 and immunoblotting 1/1000; phospho- EzrinT567, rabbit polyclonal (abcam ab47293) immunofluorescence 1/500 and immunoblotting 1/2000; p-MLC S19, mouse monoclonal and pp-MLC Thr18, S19 rabbit polyclonal (Cell Signaling Technology 3675 and 3674) immunofluorescence 1/100 and 1/200, respectively, and immunoblotting 1/1000; SLK, goat polyclonal (Santa Cruz Biotechnology sc-79068) immunofluorescence 1/100 and immunoblotting 1/1000; NHERF1/EBP50, rabbit polyclonal (Santa Cruz Biotechnology sc-134485) immunofluorescence 1/100 and immunoblotting 1/1000; p114RhoGEF, mouse monoclonal (GeneTex GTX629806) immunoblotting 1/1000; p114RhoGEF, rabbit polyclonal (GeneTex GTX102223) immunofluorescence 1/50. An affinity-purified rabbit polyclonal was used for ZO-1, immunofluorescence 1/400 [41-43]. Phalloidin-Atto 647 reagent was obtained from Sigma Aldrich and diluted 1/1000 (65906). Affinity-purified and cross-adsorbed Alexa488-, Cy3- and Cy5-labelled donkey anti-mouse, rabbit, and goat secondary antibodies were from Jackson ImmunoResearch Laboratories (1/300 diluted from 50% glycerol stocks). Affinity-purified HRP-conjugated goat anti mouse and rabbit, and donkey anti goat secondary antibodies 1/5000 were also from Jackson ImmunoResearch Laboratories (1/5000 diluted from 50% glycerol stocks). For immunofluorescence analysis cells and tissues were mounted using Prolong Gold antifade reagent (Life technologies P36930) and imaging was performed using Zeiss 700 and 710 confocal microscopes and a 64x oil lens/NA1.4. Images were processed using Zeiss Zen 2009 and Adobe Photoshop CS5 and 10 software. Co-immunoprecipitation and immunoblotting was carried out using methods previously described and were repeated at least three times[19].

Rho GTPase activity assays

For FRET experiments, cells were plated into ibid multi-well chamber slides and then transfected with pRaichu-RhoA or pRaichu-Cdc42 (kindly provided by M. Matsuda, Osaka University, Japan)[44]. The FRET analysis was performed at 37°C with a Nikon Eclipse Ti-E inverted microscope equipped with excitation and emission CFP and YFP filters in external filter wheels and using a CFI Apochromat Nano-Crystal 60x oil lens (N.A., 1.2). Crossover between CFP and YFP filters was calibrated by imaging CFP and YFP expressed alone using all four emission/excitation filter combinations. FRET efficiency maps were then produced with the Nikon software and quantified with ImageJ. The plasmid encoding the GFP-RhoA-rGBD construct was obtained from addgene and was described previously[28].

Mammalian electron microscopy

Cells were fixed and cut and mounted for scanning electron microscopy as previously described[19]. Samples were analysed in a Sigma Field Emission scanning electron microscope (Carl Zeiss) operating at 5kV. Digital images were recorded using Carl Zeiss (SmartSEM) software.

***Drosophila* strains and genetics**

Flies were maintained at 25°C on standard food. To generate whole mutant eyes, the EGUF/GMRhid system was used[45] in combination with the *gek*^{NP5192} and *gek*^{omb1080}alleles [25]. Canton S flies were used as control. Mosaic *gek* retinas where generated using the following genotype: *eyflp ; FRT42D Ubi-myrRFP / FRT42D gek.* Rescue experiments were performed using the the MARCM technique[46] combined to the *sqh-Sqh*^{E20,21} transgene [47]. The following genotype was examined: *hsFLP,Tubulin-Gal4, nuGFP/+ ; FRT42D, TubGal80/ FRT42, gek*^{NP5192} *; sqh-Sqh*^{E20E21}*/+*. Pupal retinas where staged and stained according as described[48].

***Drosophila* antibodies and immunological methods**

Whole mount retinas were prepared as described in[48]. The following antibodies were used: rabbit anti-p-MLC Ser19, 1/40 (Cell Signaling Technology 3671); rabbit anti-PKCζ 1/200 (Sigma Aldrich SAB4502380), mouse anti-Arm 1/200 (N27-A1, Developmental Studies Hybridoma Bank), rabbit anti-Gek 1/25 (gift from TR Clandinin[25], rabbit anti-P-Moesin 1/500[49], phalloidin-Texas Red (Sigma Aldrich, 300nM) with the appropriate combination of secondary antibodies conjugated to Dy405, Alexa488, Cy3 or Cy5 as appropriate at 1/200 each (Jackson ImmunoResearch). Retinas were mounted in VectaShield and imaging was performed using a Leica SP5 confocal. Images were processed using ImageJ and Adobe Photoshop 7.0.

***Drosophila* electron microscopy**

Electron microscopy was performed as in[50] using a Tecnai G2 Spirit transmission electron microscope (FEI, The Netherlands) equipped with a Morada CCD camera (Olympus Soft Imaging Systems). Image quantification was performed using iTEM software.

Statistics and reproducibility

Mammalian epithelial cells - Microvilli induction was measured as cluster areas since clusters represent advanced microvilli induction during differentiation that proceeds initial

bud formation at the early stage of differentiation[51]. Cluster areas were measured in scanning electron micrographs using Nikon Imaging software (NIS) (Supplementary Figure 1) by determining threshold intensity. 2-3 areas of each cell at a magnification of 40,000x were measured to accommodate cluster variation in each cell. Cell height was measured in Zeiss 700 confocal Z-sections using Zeiss Zen2000 imaging software. Co-localisation coefficients were calculated with the Zeiss 700 microscope software. Cell height was measured using basal and apical markers and at 3μM intervals to accommodate for variation of height along individual cells, and values were then averaged. p-MLC (ser19), F-actin, EFP-LA, polarity and brush border protein pixel intensity was measured using Image-J software. For each cell background was measured and subtracted from the sample value. Co-localization coefficients were measured in Zeiss Confocal XY or Z-scans using Zeiss Zen 2000 co-localization software that applies the principal of the Pearson's coefficient, using cross-hairs facility to subtract background from each channel. For the quantifications shown, the provided n values refer to independent experiments and the numbers in the graphs refer to the total of analysed cells per type of sample across all experiments. Statistical significance was tested in most experiments using two-tailed Student's t-tests, pairing values derived from the same experiment. The FRET experiments are shown as standard box plots (25th to 75th percentiles, with a line at the median; whiskers extend to the max/min data points) and were analysed with a nonparametric Mann-Whitney-Wilcoxon test. The experiments that were not quantified in figures1b, 3e and f, and 7c, as well as supplementary figures 3e, 5b, 6e and 7c are representative for 3 experiments. Localization of MRCK in mouse tissue was analysed in sections derived from 2 different animals (figure 4d). Graphs and statistical calculations were generated using MS Excel (V15) and JMP (V12).

Drosophila - Pixel intensity/membrane length measurements of apical membrane and Arm domains were determined by analysing confocal images of *gek* mosaic retinas at 40% APF using ImageJ. A minimum of four independent retinas were used for each genotype. Parametric samples were tested for statistical significance using paired two-tailed Student's t-test. The numbers of animals analysed: figure 2b-d, n=11; figure 2e,f, n=4 for each genotype; figure 2g,h, n=8; figure 4e, n=8; figure 6, n=4 (i); n=6 (j); figure 8, n=10 (k), n=8 (l), n=7 (m), n=7 (n); and Supplementary figure 9 n=9 (a), n=7 (b), and n=7 (c,d), n=7 .

Data availability

All data supporting the conclusions here are available from the authors on reasonable request.

38. Matter, K., Brauchbar, M., Bucher, K. & Hauri, H.P. Sorting of endogenous plasma membrane proteins occurs from two sites in cultured human intestinal epithelial cells (Caco-2). *Cell* **60**, 429-437 (1990).
39. Matter, K., Hunziker, W. & Mellman, I. Basolateral sorting of LDL receptor in MDCK cells: the cytoplasmic domain contains two tyrosine-dependent targeting determinants. *Cell* **71**, 741-753 (1992).
40. Carlton, J.G. & Martin-Serrano, J. Parallels between cytokinesis and retroviral budding: a role for the ESCRT machinery. *Science* **316**, 1908-1912 (2007).

41. Benais-Pont, G. *et al.* Identification of a tight junction-associated guanine nucleotide exchange factor that activates Rho and regulates paracellular permeability. *J Cell Biol* **160**, 729-740 (2003).
42. Balda, M.S., Garrett, M.D. & Matter, K. The ZO-1-associated Y-box factor ZONAB regulates epithelial cell proliferation and cell density. *J Cell Biol* **160**, 423-432 (2003).
43. Sourisseau, T. *et al.* Regulation of PCNA and cyclin D1 expression and epithelial morphogenesis by the ZO-1-regulated transcription factor ZONAB/DbpA. *Mol Cell Biol* **26**, 2387-2398 (2006).
44. Yoshizaki, H. *et al.* Activity of Rho-family GTPases during cell division as visualized with FRET-based probes. *J Cell Biol* **162**, 223-232 (2003).
45. Stowers, R.S. & Schwarz, T.L. A genetic method for generating Drosophila eyes composed exclusively of mitotic clones of a single genotype. *Genetics* **152**, 1631-1639 (1999).
46. Lee, T. & Luo, L. Mosaic analysis with a repressible cell marker for studies of gene function in neuronal morphogenesis. *Neuron* **22**, 451-461 (1999).
47. Winter, C.G. *et al.* Drosophila Rho-associated kinase (Drok) links Frizzled-mediated planar cell polarity signaling to the actin cytoskeleton. *Cell* **105**, 81-91 (2001).
48. Walther, R.F. & Pichaud, F. Immunofluorescent staining and imaging of the pupal and adult Drosophila visual system. *Nat Protoc* **1**, 2635-2642 (2006).
49. Karagiosis, S.A. & Ready, D.F. Moesin contributes an essential structural role in Drosophila photoreceptor morphogenesis. *Development* **131**, 725-732 (2004).
50. Pinal, N. *et al.* Regulated and polarized PtdIns(3,4,5)P3 accumulation is essential for apical membrane morphogenesis in photoreceptor epithelial cells. *Curr Biol* **16**, 140-149 (2006).
51. Crawley, S.W., Mooseker, M.S. & Tyska, M.J. Shaping the intestinal brush border. *J Cell Biol* **207**, 441-451 (2014).

Supplementary Figure 1

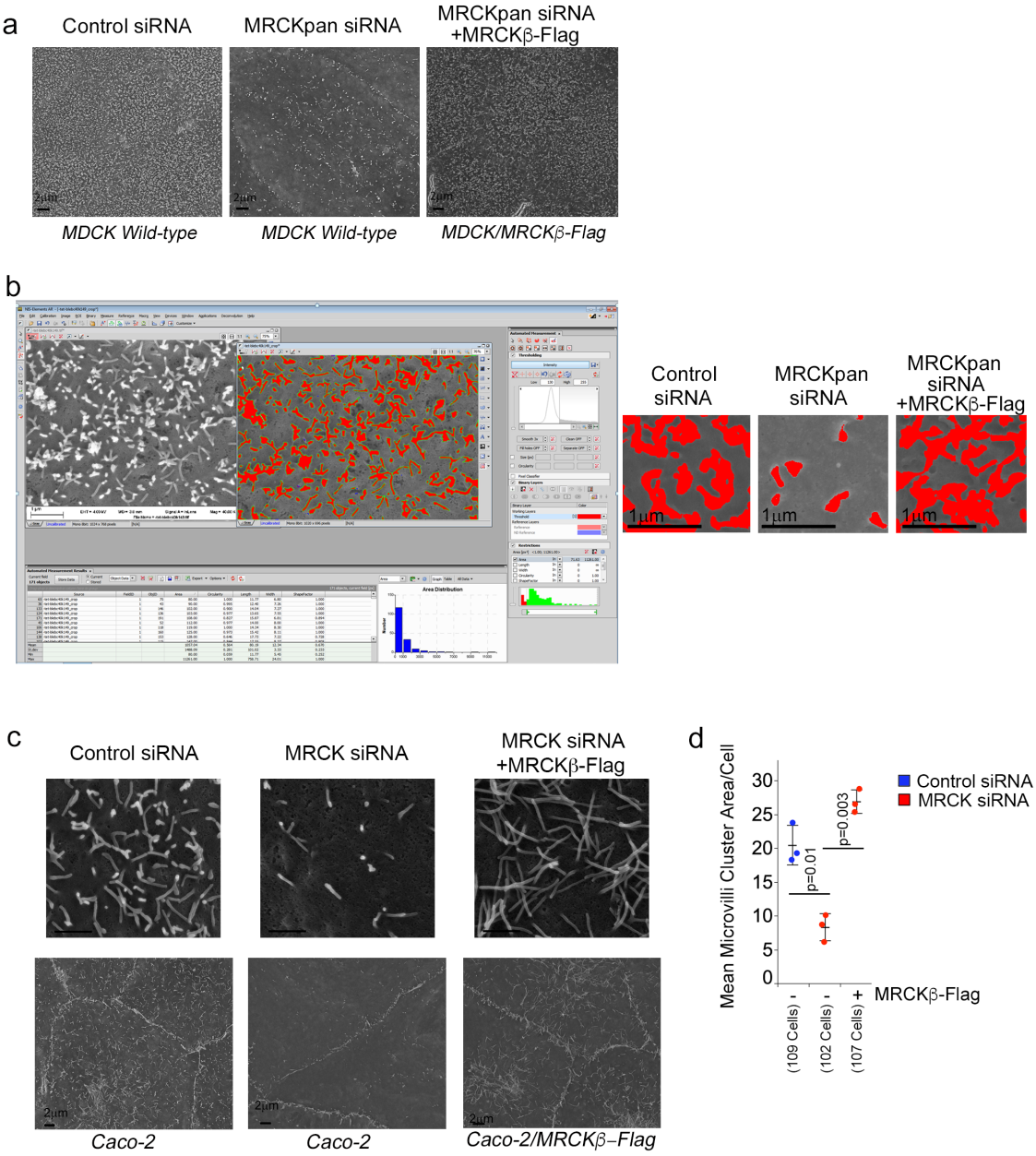

Supplementary Figure 1: Quantification of microvilli induction and role of MRCK in apical morphogenesis of Caco-2 cells. (**a**) Broad view of apical surface of MDCK cells by scanning electron microscopy after MRCK knockdown and after complementation with MRCKβ-flag. (**b**) Measurement of apical membrane brush border cluster induction using threshold function of Nikon imaging software. (**c,d**) Levels of microvilli induction in human Caco-2 intestinal epithelial cells following MRCK knockdown without or with complementation with MRCKβ-flag. Panel d is based on n=3 independent experiments and shows the data points, means ± 1 SD (in black), the total number of cells analysed for each type of sample across all experiments, and p-values derived from t-tests.

Supplementary Figure 2

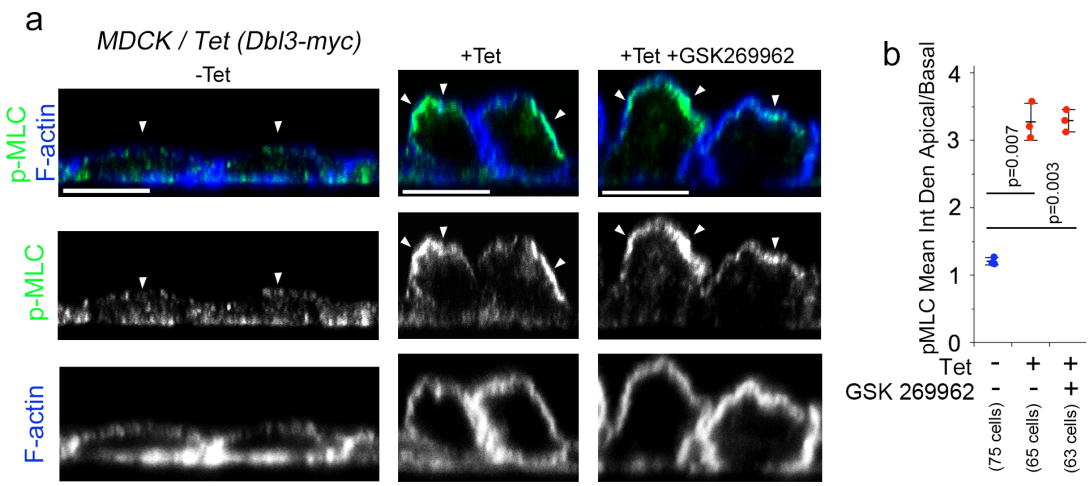

Supplementary Figure 2: Inhibition of ROCK does not affect Dbl3-induced apical actomyosin activation. Confocal analysis of apical pMLC activity and F-actin in MDCK cells upon induction of Dbl3 expression by tetracycline in a conditional cell line in the absence or presence of the ROCK inhibitor GSK269962. Arrowheads point to apical cortex. Panel b is based on n=3 independent experiments and shows the data points, means ± 1 SD (in black), the total number of cells analysed for each type of sample across all experiments, and p-values derived from t-tests. Scale bars: 10 µm.

Supplementary Figure 3

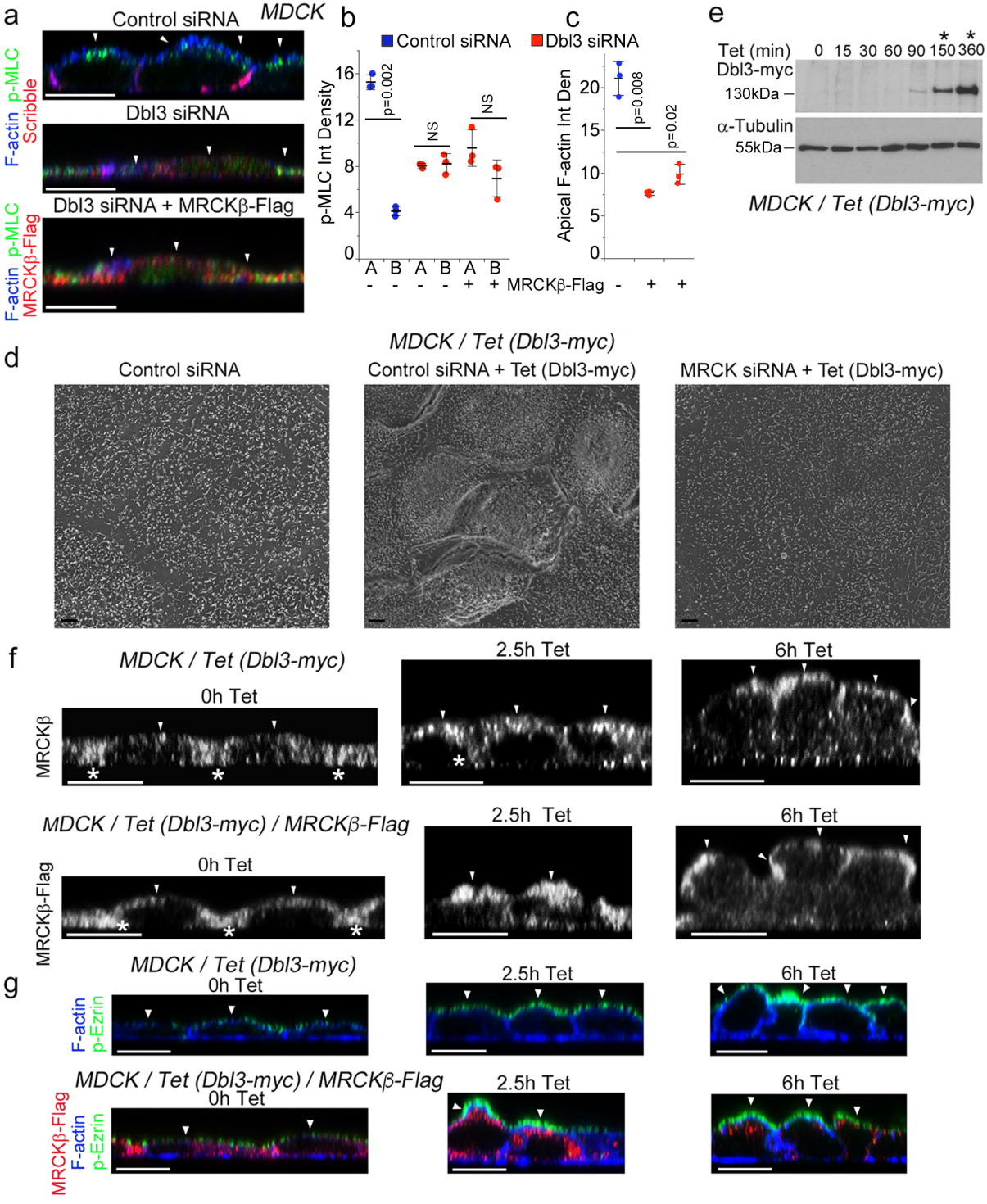

Supplementary Figure 3: MRCKβ expression does not rescue loss of apical Myosin-II activation and differentiation in Dbl3-depleted MDCK cells: (**a-c**) Levels of Myosin phosphorylation at the apical membrane domain (A) and basal membrane (B) and F-actin during polarization and differentiation of MDCK cells following Dbl3 siRNA transfection and with constitutive expression of MRCKβ-flag. Quantifications are based on n=3 independent experiments and show the data points, means ± 1 SD (in black), the total number of cells analysed for each type of sample across all experiments, and p-values derived from t-testsshow means ± 1 SD, n+3. (**d**) SEM images of the effect of MRCK knock down on

microvilli induction and conditional expression of Dbl3-myc. Note, MRCKβ-flag does not rescue the Dbl3 depletion-induced phenotype. (**e**) Time course of tetracycline-induced Dbl3-myc expression in MDCK cells. Asterisks highlight time points with clear induction of Dbl3-myc expression that were used for the functional assays. Unprocessed original scans of blots are shown in Supplementary Figure 8. (**f**) Confocal z-sections showing representative images of either endogenous or constitutively expressed MRCKβ in MDCK cells following conditional tetracycline-inducible expression of Dbl3-myc. Constitutive expression of MRCKβ-flag accelerates activation of Myosin-II at the apical membrane, highlighted by white arrows. Asterisks highlight basolateral MRCK localization at earlier stages of polarization. (**g**) Confocal Z-sections showing representative images of pEzrinT567 localization in MDCK cells following conditional tetracycline-inducible expression of Dbl3-myc without or with constitutive expression of MRCKβ-flag. Constitutive expression of MRCKβ-flag accelerates enrichment of active Ezrin at the apical membrane domain, indicated by white arrowheads. Scale bars: 10 μm.

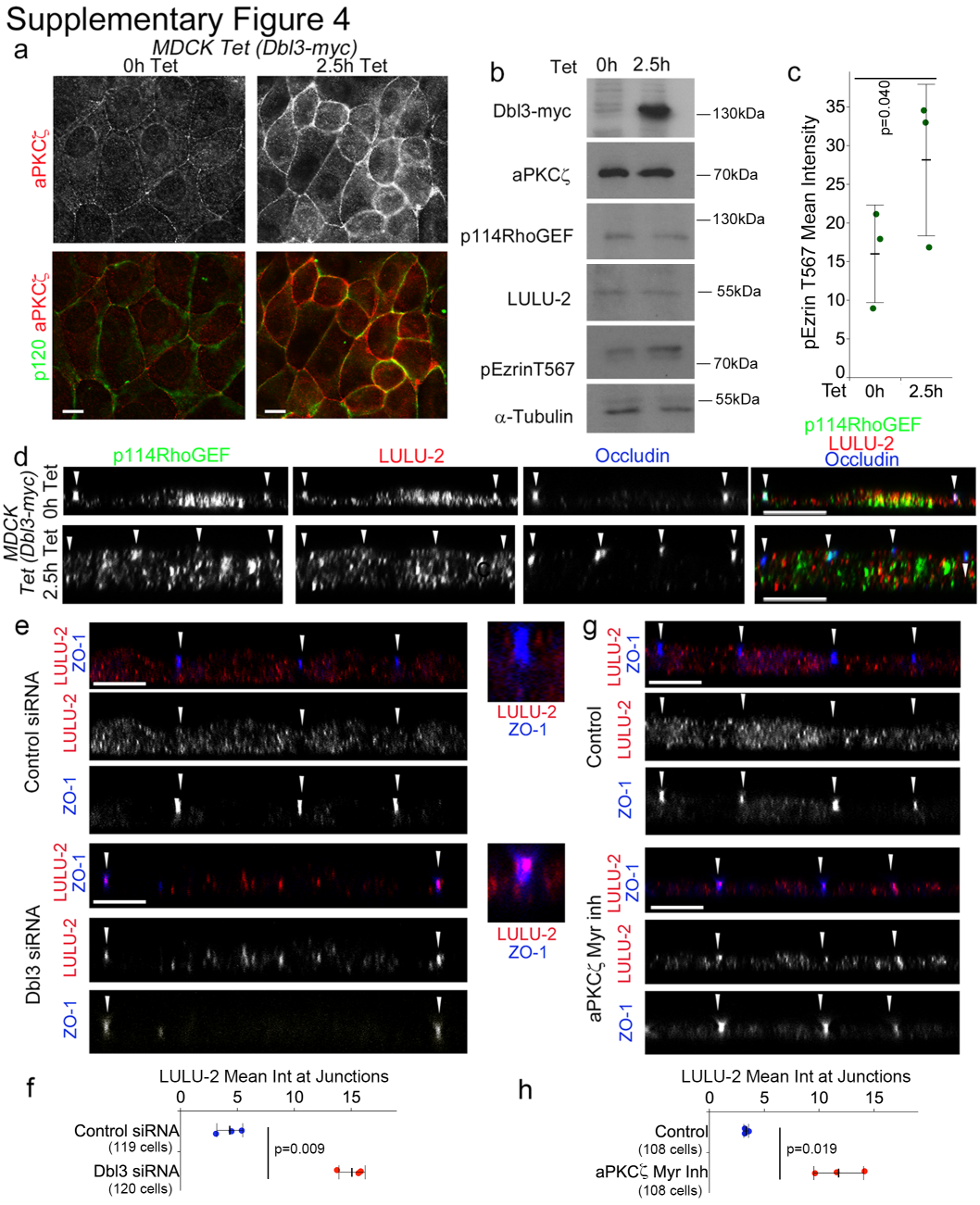

Supplementary Figure 4: Cdc42 stimulates aPKC recruitment and antagonizes Rho-signalling. (**a**) Conditional tetracycline-induced expression of Dbl3 in MDCK cells stimulates increased recruitment of aPKCζ . Shown are confocal xy. (**b**) Levels of protein expression during tetracycline-induced Dbl3-myc expression. Unprocessed original scans of blots are shown in Supplementary Figure 8. (**c**) Quantification of levels of pEzrinT567D following tetracycline-induced Dbl3-myc expression. (**d**) Conditional tetracycline-induced expression of Dbl3 in MDCK cells stimulates loss of junctional p114RhoGEF and LULU-2. Shown are confocal z-sections. Junctions are indicated with white arrowheads. (**e,f**) Spontaneously polarizing MDCK cells were treated with control or Dbl3 siRNAs, or a myristoylated aPKCζ inhibitor. LULU-2 localization at tight junctions was then analysed by confocal microscopy using ZO-1 as a marker for tight junctions (indicated by arrowheads). Quantifications are based on n=3 independent experiments and show the data points, means ± 1 SD (in black), the total number of cells analysed for each type of sample across all experiments, and p-values derived from t-tests. Scale bars: 10 µm.

Supplementary Figure 5

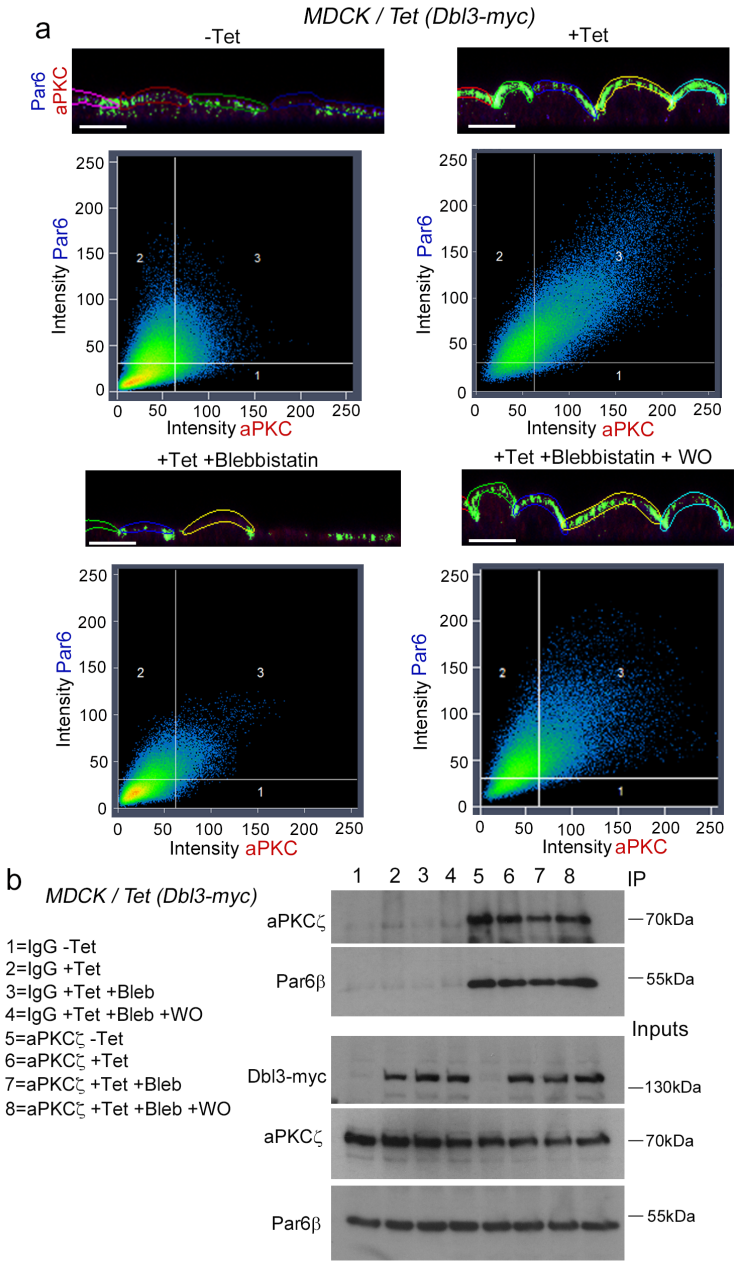

Supplementary Figure 5: MRCK-activated Myosin-II motor activity drives apical polarization of Par6-aPKC complex. (**a**) MDCK cells conditionally expressing tetracycline-inducible Dbl3-myc were analysed by confocal microscopy using co-localization software based on the Pearson's correlation coefficient. Co-localization is calculated in grid 3 of the scatter charts. Bright green represents co-localization of aPKCζ and Par6β, which increases and is confined to the apical cortical membrane following polarization stimulated by conditional tetracycline inducible Dbl3-myc expression in MDCK cells and is dependent on Myosin-II motor activity. Coloured outlines of apical membrane domains represent calculation areas of co-localization coefficients. Scale bars: 10µm. (**b**) Co-immunoprecipitation of Par6 and aPKC indicating formation of stable complexes that are independent of Myosin-II motor activity and Dbl3 expression. Unprocessed original scans of blots are shown in Supplementary Figure 8.

Supplementary Figure 6

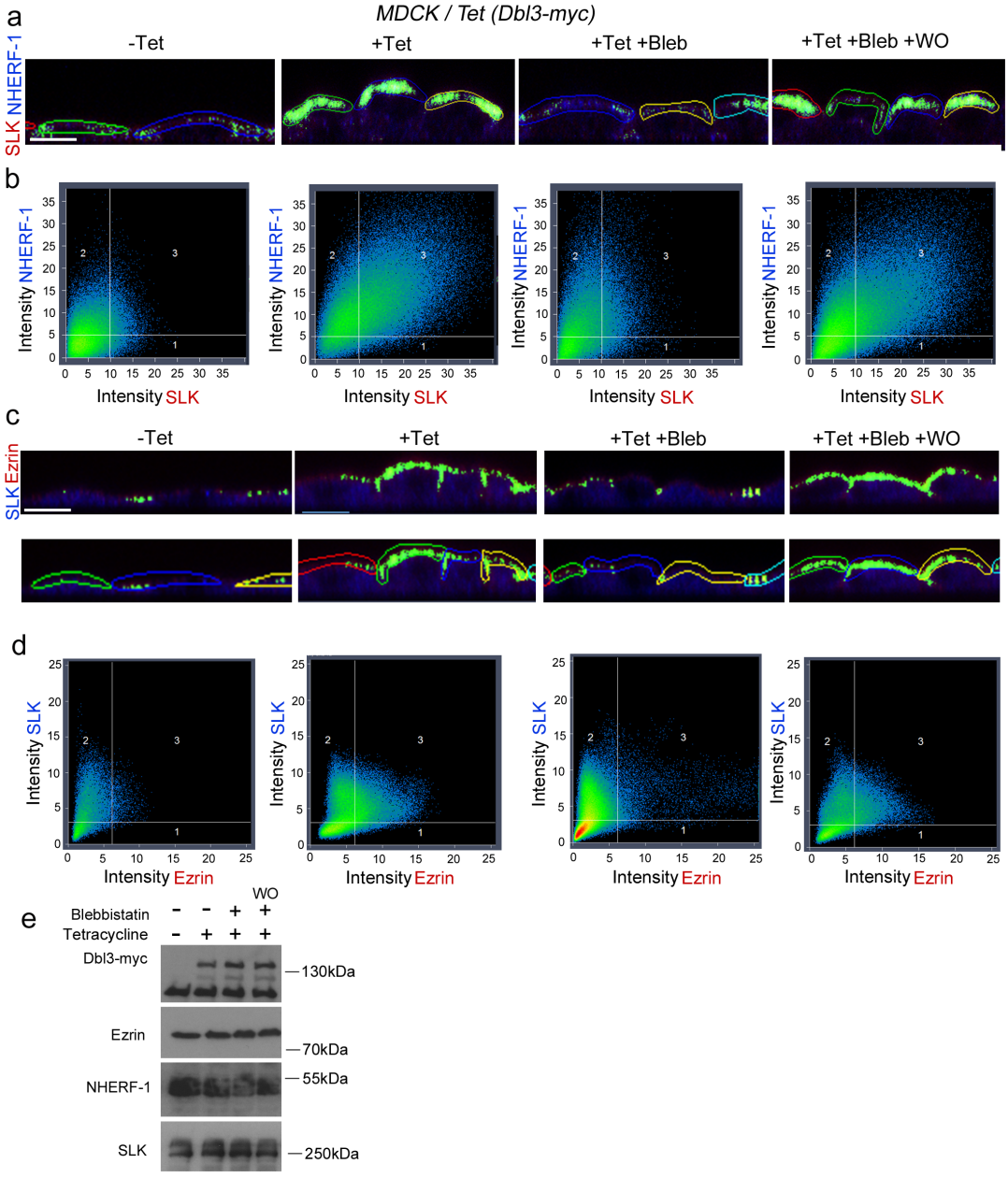

Supplementary Figure 6: Dbl3-activated Myosin-II motor activity drives apical polarization and co-localization of brush border regulators. (**a-d**) MDCK cells conditionally expressing tetracycline-inducible Dbl3-myc were analysed by confocal microscopy using co-localization software based on the Pearson's correlation coefficient. Co-localization is calculated in grid 3 of the scatter charts. Bright green represents co-localization of Ezrin and SLK or NHERF-1 and SLK, which increases and is confined to the apical membrane domain following polarization stimulated by conditional tetracycline inducible Dbl3-myc expression in MDCK cells and is dependent on Myosin-II motor activity. Coloured outlines of apical membrane domains represent calculation areas of co-localization coefficients. Scale bars: 10µm. (**e**) Expression levels of differentiation markers upon Dbl3 and Myosin manipulation. Unprocessed original scans of blots are shown in Supplementary Figure 8.

Supplementary Figure 7

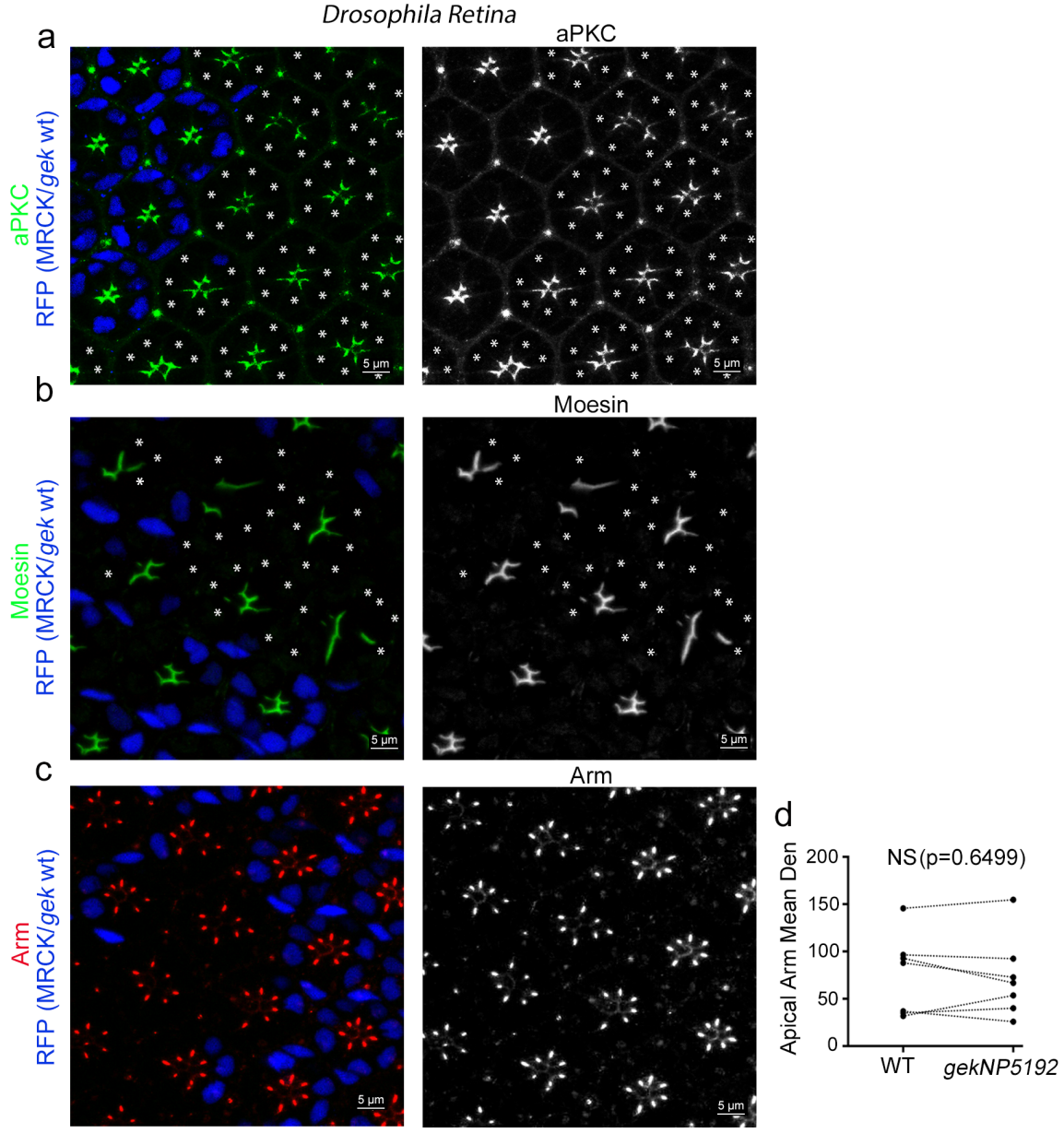

Supplementary Figure 7: Myosin-II activation mediates *gek* function in pupal photoreceptors. (**a-c**) Confocal sections of a pupal retinas showing wild type cells (blue nuclei) and *gek* mutant cells (labelled with asterisks) stained for the apical markers aPKC and Moesin, or the junctional marker Arm. (**d**) Quantification of the effect of mutant *gek* on junctional levels of Arm (measurements from wild type and neighbouring mutant cells, paired within sections; based on n=7 animals; p value was calculated with a t-test).

Figure 1b

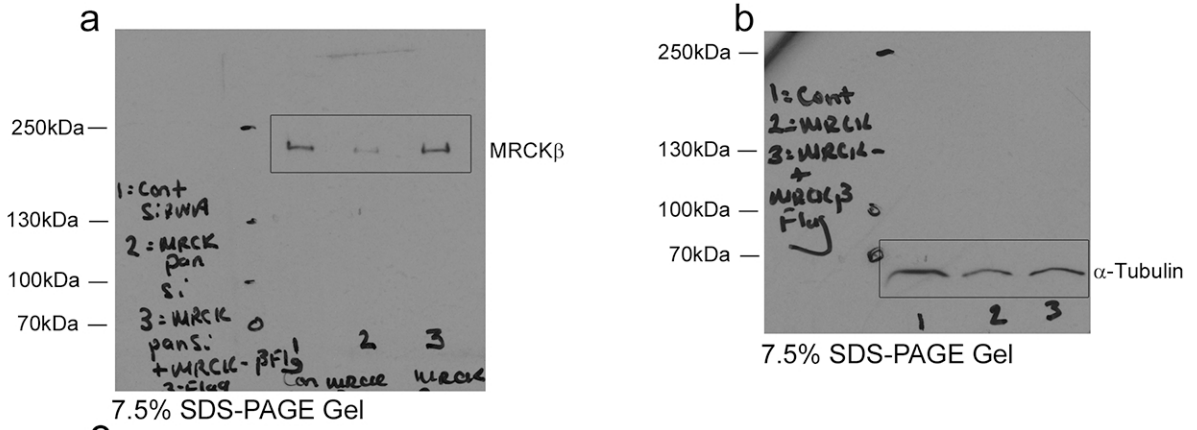

7.5% SDS-PAGE Gel

7.5% SDS-PAGE Gel

Figure 3e

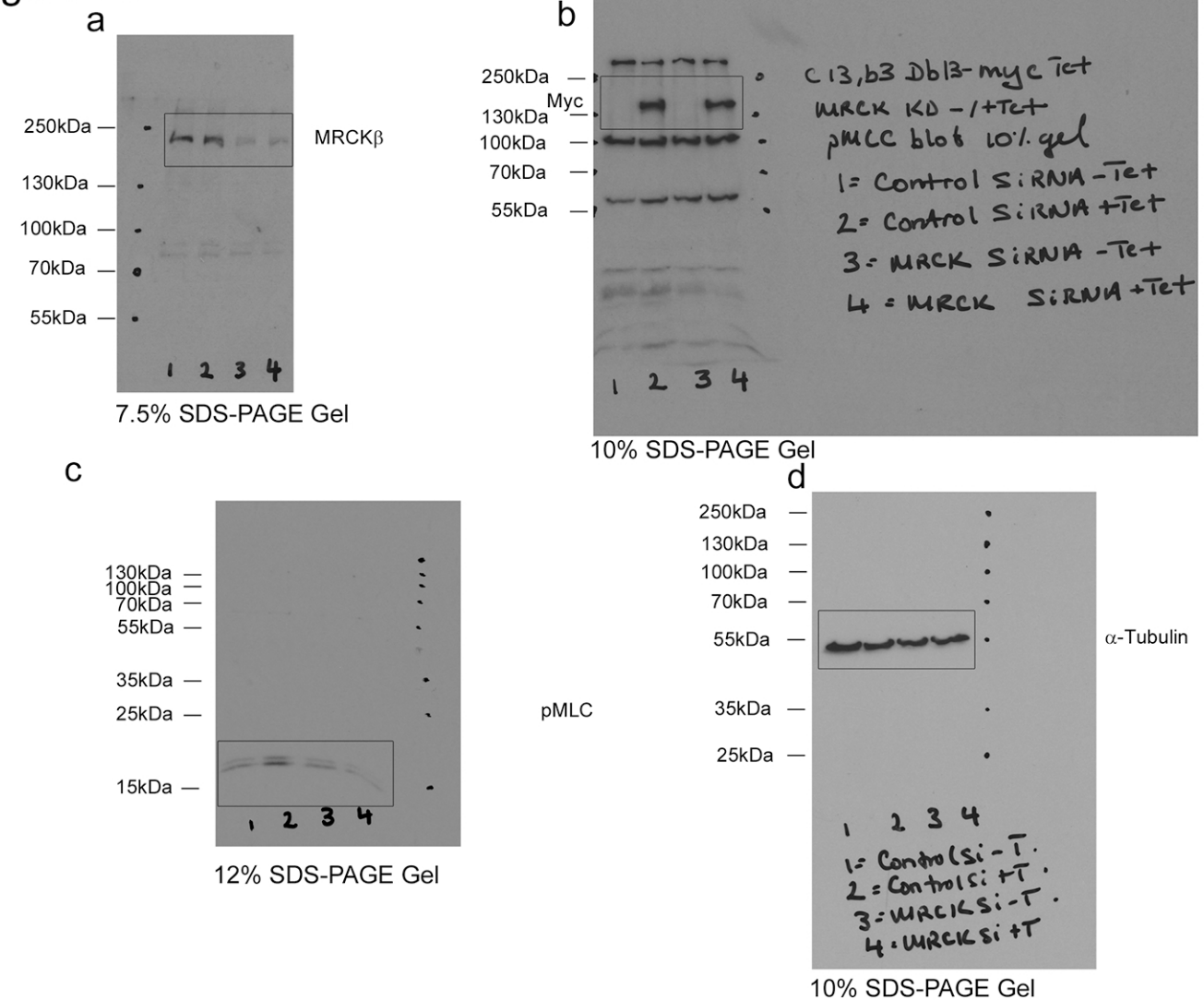

7.5% SDS-PAGE Gel

10% SDS-PAGE Gel

12% SDS-PAGE Gel

10% SDS-PAGE Gel

Figure 3f

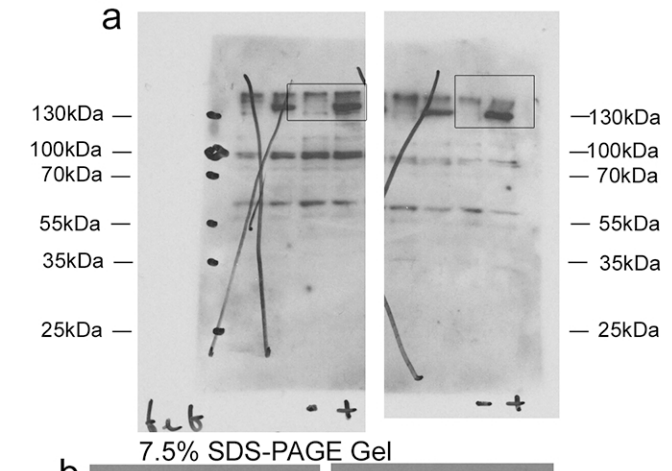

Figure 7c

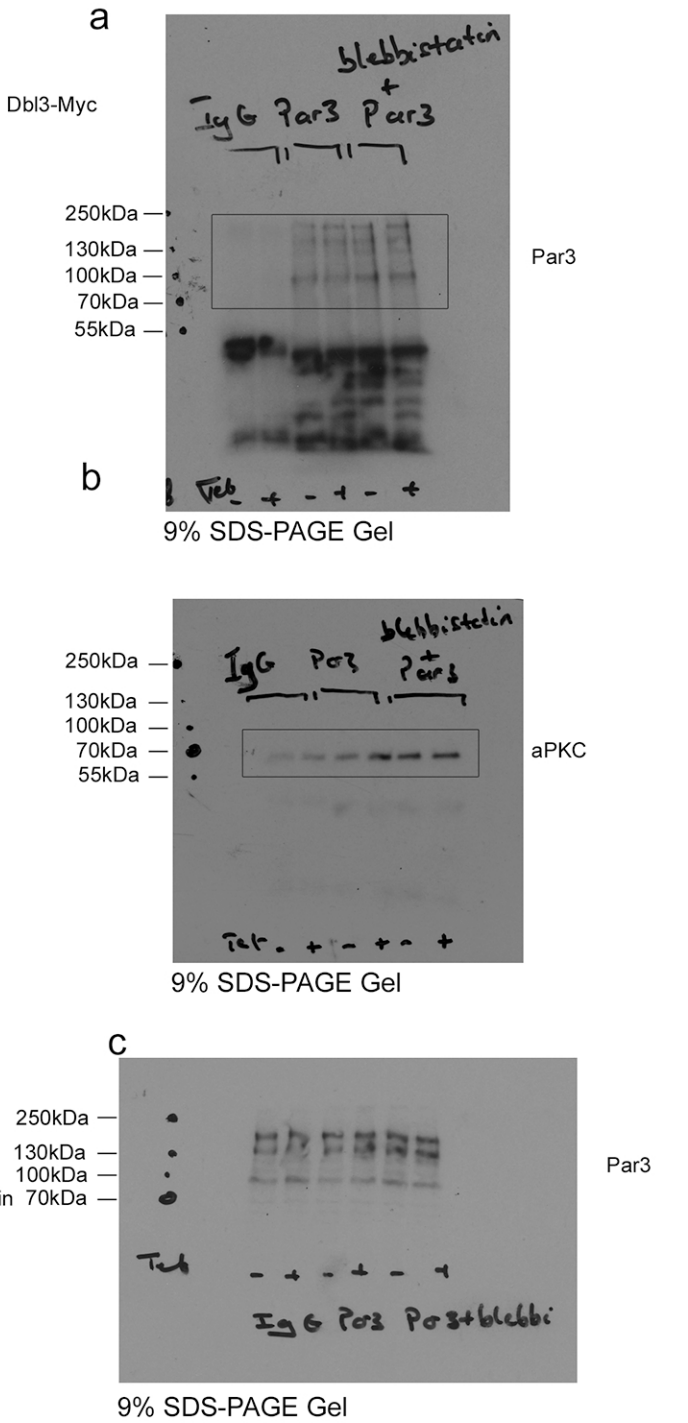

Figure 7c Cont'd

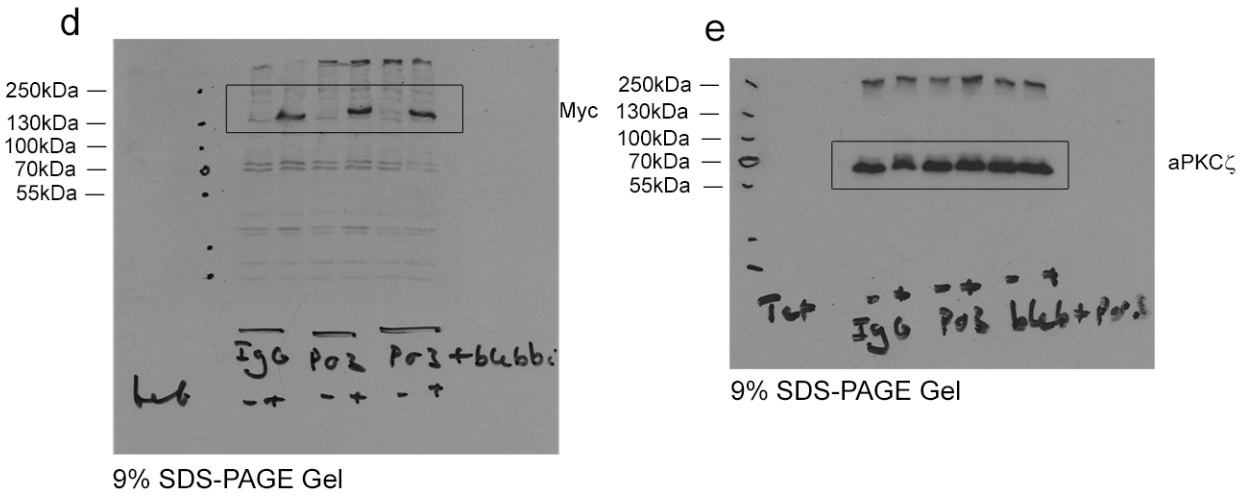

Supplementary Figure 3e

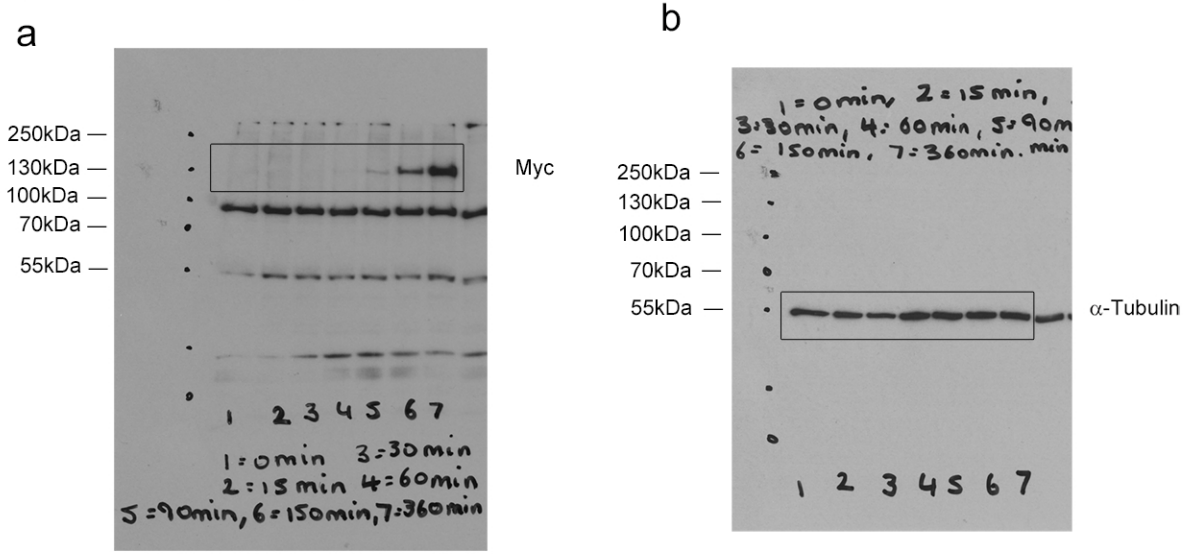

Supplementary Figure 4b

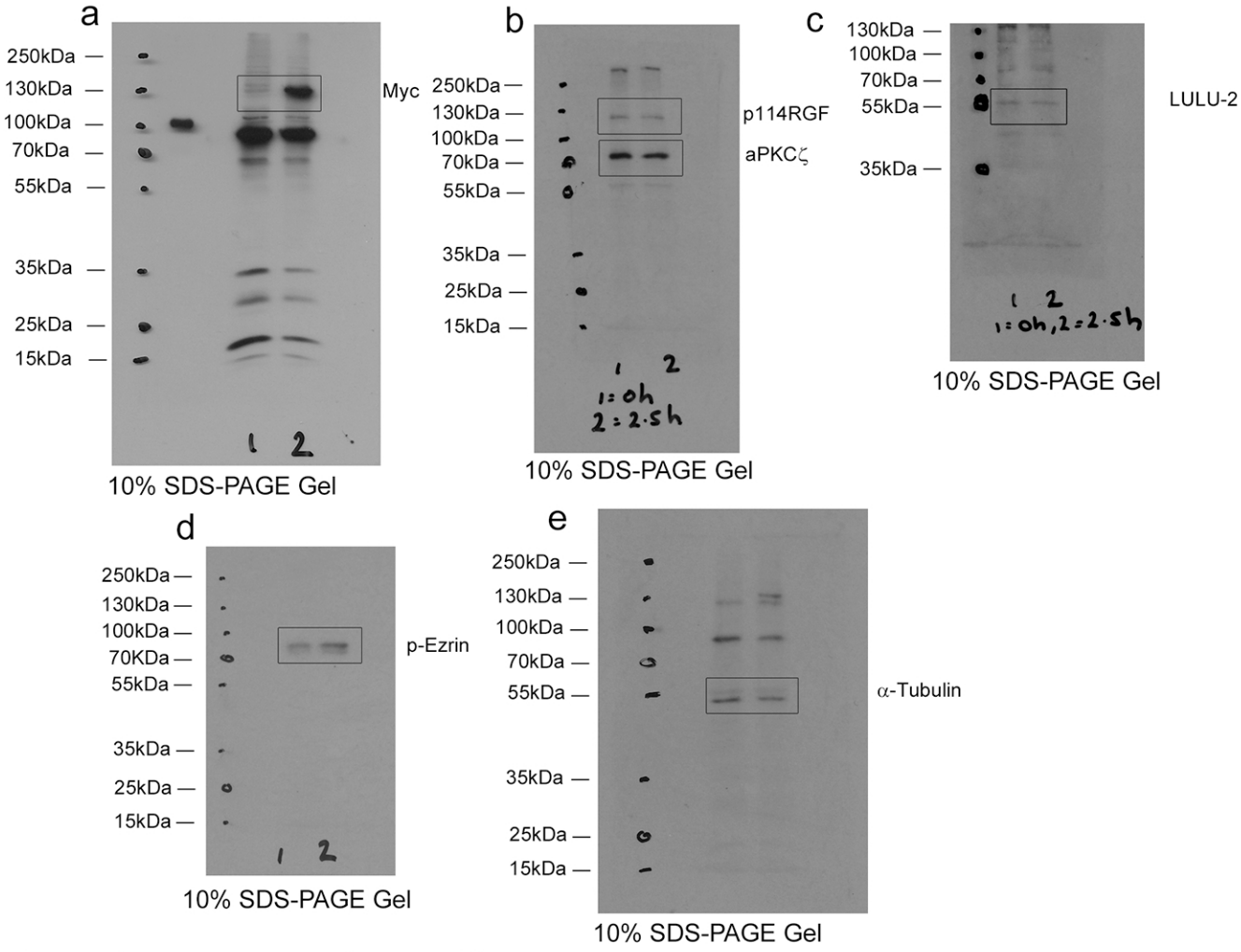

Supplementary Figure 5b

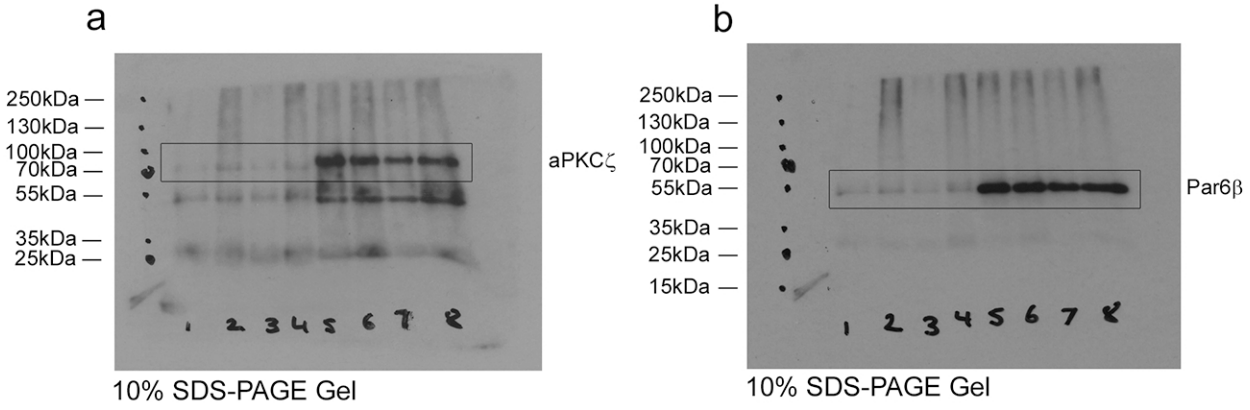

Supplementary Figure 5b Cnt'd

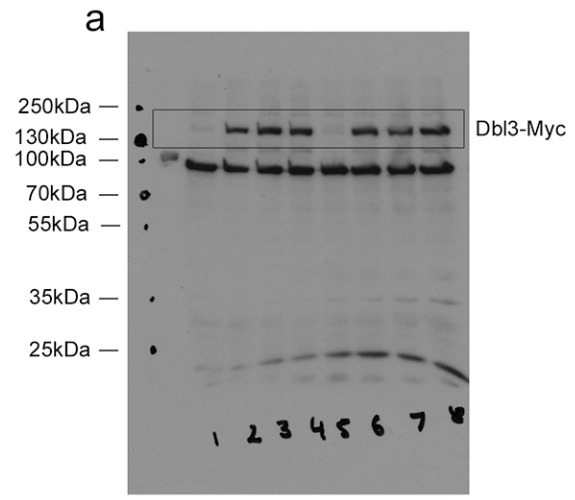

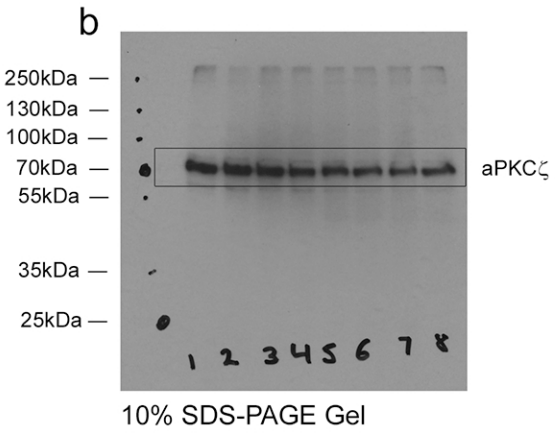

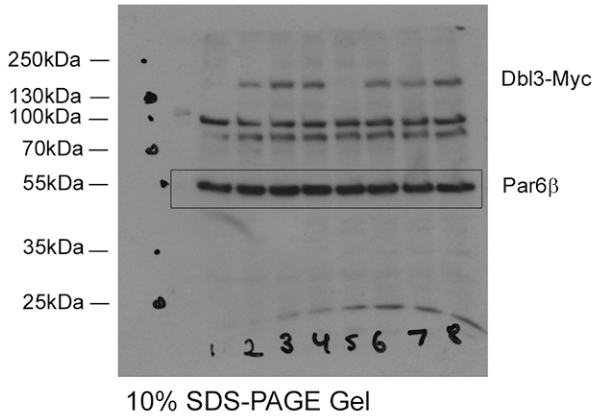

Supplementary Figure 6e

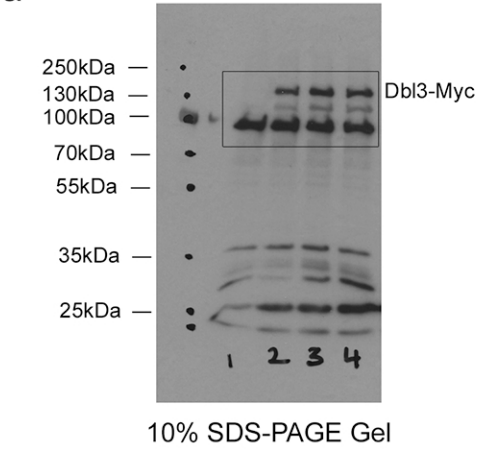

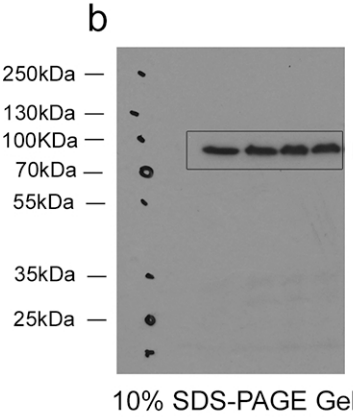

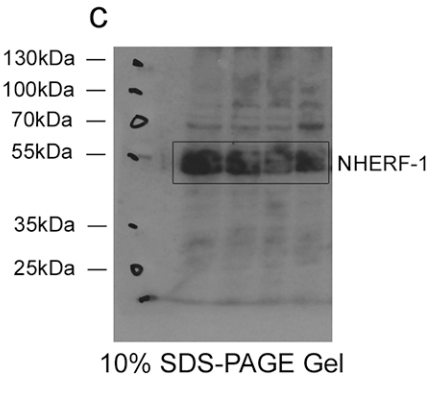

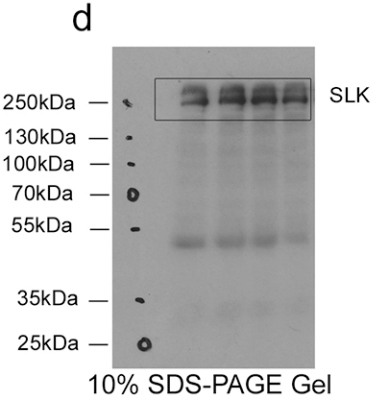

Information about antibody sources						
Antigen	**Provider**	**Catalogue Number**	**Batch Number**	**Description**	**Specificity**	**Validation**
EHMD/Lulu-2	abcam	ab77484	GR77589-1	goat polyclonal	Recognises a long and a short form of Lulu-2 in human and canine cells	Immunoblotting and peptide quenching (http://www.abcam.com/ehm2-antibody-ab77484.html) and by siRNA-mediated depletion (JCB 195, 245-61, 2011)
Par3	Millipore	07-330	216672, DAM1754440	rabbit polyclonal	Recognises multiple Par3 isoforms in human and canine cells	Immunoblotting human and mouse total cell extracts (http://www.merckmillipore.com/GB/en/product/Anti-Partitioning-defective-3-Antibody,MM_NF-07-330?ReferrerURL=https%3A%2F%2Fwww.google.co.uk%2F&bd=1) and immunoprecipitation of MDCK cell extracts and immunofluorescence of MDCK cells (JCB
PARβ2	Santa Cruz Biotechnology	sc-67392	K2613, A0809, A2108	rabbit polyclonal H-64	Recognises human and canine PARβ2	Immunoblotting, immunoprecipitation and immunofluorescence of MDCK and Caco-2 cells (JCB 204, 111-27, 2014) and immunoblotting total cell extracts from different species (https://www.scbt.com/scbt/product/pard3b-antibody-h-64)
PKCζ	Santa Cruz Biotechnology	sc-17781	G0212, E2014	mouse monoclonal H-1	Recognises human, canine and rodent aPKCζ	Immunoblotting of total cell extracts and immunocytochemistry of human tissue sections (https://www.scbt.com/scbt/product/pkc-zeta-antibody-h-1) as well as immunofluorescence of MDCK cells (JCB 204, 111-27, 2014)
Occludin	InvitrogenThermoFisher Scientific	331560	1031631A	mouse monoclonal OC-3F10	Recognises human, mouse and canine occludin	Immunoblotting and immunofluorescence of MDCK and Caco-2 cells (https://www.thermofisher.com/antibody/product/Occludin-Antibody-clone-OC-3F10-Monoclonal/33-1500 and BMC Cell Biol 10, 95, 2009)
Scribble	Santa Cruz Biotechnology	sc-11049	F0816	goat polyclonal C-20	Recognises human and canine Scribble	Immunofluorescence and immunoblotting in human and canine epithelial cells (https://www.scbt.com/scbt/product/scrib-antibody-c-20 and JCB 204, 111-27, 2014)
MRCKβ	Santa Cruz Biotechnology	sc-48834	J2609	rabbit polyclonal H-125	Recognises human, mouse and canine MRCKβ	Immunoblotting and immunofluorescence of MDCK and Caco-2 cells, and by siRNA-mediated depletion (http://www.scbt.com/ex/datasheet-48834-mrckbeta-h-125-antibody.html and this manuscript)
Ezrin	Santa Cruz Biotechnology	sc-58758	E0710	mouse monoclonal 3C12	Recognises human and canine ezrin	Immunoblotting and immunofluorescence, and by siRNA-mediated depletion (https://www.scbt.com/scbt/product/ezrin-antibody-3c12 and JCB 204, 111-27, 2014)
phospho-Ezrin T567	abcam	ab47293	803415	rabbit polyclonal	Recognises ezrin phosphorylated at Thr567 in different vertebrate species	Immunoblotting cell extracts after different stimuli promoting phosphorylation and peptide quenching (http://www.abcam.com/ezrin-phospho-t567-antibody-ab47293.html#description_images_1 and Nat Comm 6, 8871, 2015)
phospho-MLC S19	Cell Signaling Technology	3675	1	mouse monoclonal	Recognises MLC phosphorylated at Ser19 in different species	Immunoblotting of control and phosphase treated cell extracts and by immunofluorescence (https://www.cellsignal.com/products/primary-antibodies/phospho-myosin-light-chain-2-ser19-mouse-mab/3675)
phospho(pp)MLC T18, S19	Cell Signaling Technology	3674	5	rabbit polyclonal	Recognises MLC phosphorylated at Thr 18 and Ser19 in different species	Immunoblotting control and stimulated cell extracts and by immunofluorescence staining of human epithelial cells (https://www.cellsignal.com/products/primary-antibodies/phospho-myosin-light-chain-2-thr18-ser19-antibody/3674 and Nat Cell Biol 13, 159-66, 2011)
phospho-MLC S19	Cell Signaling Technology	3971	3	rabbit polyconal	Recognises MLC phosphorylated at Ser19 in different species including	Immunoblotting and immunofluorescence ionophore-stimulated cells (https://www.cellsignal.com/products/primary-antibodies/phospho-myosin-light-chain-2-ser19-antibody/3671 and Develop 139, 3432-41, 2012)
SLK	Santa Cruz Biotechnology	sc-79068	B2410	goat polyclonal C-18	Recognises human and canine SLK	Immunoblotting and immunofluorescence of human and canine cells (https://www.scbt.com/scbt/product/slk-antibody-c-18 and this manuscript)
NHERF1/EBP50	Santa Cruz Biotechnology	sc-134485	H2313	rabbit polyclonal H-300	Recognises NHERF1 of various vertebrate species	Immunoblotting and immunofluorescence of human and canine cells (https://webcache.googleusercontent.com/search?q=cache:Uc3dFYCjCBsJ:https://www.scbt.com/scbt/product/nherf-1-antibody-h-300+&cd=2&hl=en&ct=clnk&gl=uk&client=firefox-b and this manuscript)
PKCζ	Sigma Aldrich	SAB4502380	210805	rabbit polyconal	Recognises PKCζ in multiple species	Immunoblotting and immunofluorescence (http://www.sigmaaldrich.com/catalog/product/sigma/sab4502380?lang=en&region=GB)
p114RhoGEF	GeneTex	GTX628806	41449	mouse monoclonal	Recognises mammalian p114RhoGEF	Immunoblotting and immunofluorescence, and siRNA-mediated depletion (http://www.genetex.com/ARHGEF18-antibody-GTX972-GTX628806.html and JCB 195, 245-61, 2011)
p114RhoGEF	GeneTex	GTX102223	39820	rabbit polyconal	Recognises mammalian p114RhoGEF	Immunoblotting and immunofluorescence, and siRNA-mediated depletion (http://www.genetex.com/ARHGEF18-antibody-GTX102223.html and JCB 195, 245-61, 2011)
ZO-1	not commercial	not applicable	not applicable	rabbit polyclonal	Recognises vertebrate ZO-1	Immunofluorescence and immunoblotting combined with siRNA-mediated depletion (JCB 160, 729-40, 2003; Mol Cell Biol 26, 2387-98)
Arm	Developmental Studies Hybridoma Bank	N27-A1	not applicable	mouse monoclonal N27-A1	Recognises *Drosophila* Armadillo	Immunofluorescence and immunoblotting (http://dshb.biology.uiowa.edu/N2-7A1-ARMADILLO and Cell 63, 549-60, 1990)
Gek	not commercial	not applicable	not applicable	rabbit polyclonal	Recognises *Drosophila* GEK	Immunofluorescence of wild type and mutant flies (Develop 138, 4899-909, 2011)
phospho-Moesin T558	not commercial	not applicable	not applicable	rabbit polyclonal	Recognises *Drosophila* Moesin phosphorylated at Thr558	Immunofluorescence of wild type and mutant flies (Develop 131, 721-32, 2004)

Supplementary Table 1: Details of antibodies used. Information about antibody sources and specificity.

Supplementary Video 1: Induction of polarized myosin activation by Cdc42. Apical Cdc42 activation by conditional expression of Dbl3-myc in MDCK cells constitutively expressing EGFP-MLC was induced by adding tetracycline followed by recording image stacks every 5 minutes. Shown are projections of 4 images derived from the apical domain. The experiment was performed five times.